Volume 3
Number 19
7 October 2022
Pages 7145–7372

Materials Advances

rsc.li/materials-advances

ISSN 2633-5409

ROYAL SOCIETY OF CHEMISTRY

REVIEW ARTICLE
Yu-Cheng Chiu *et al.*
From stretchable and healable to self-healing semiconducting polymers: design and their TFT devices

Materials Advances

ROYAL SOCIETY OF CHEMISTRY

REVIEW

View Article Online
View Journal | View Issue

Cite this: *Mater. Adv.*, 2022, 3, 7154

From stretchable and healable to self-healing semiconducting polymers: design and their TFT devices

Livy Laysandra, Andreas Njotoprajitno, Suhendro Purbo Prakoso and Yu-Cheng Chiu *

Flexible thin-film transistor (TFT) devices are essential elements of future flexible electronics owing to their promising applications in various fields ranging from lighting and display, sensors, communication, and smart textiles to medical devices. Currently, these state-of-the-art electronic devices are not only struggling from "brittle" to "stretchable", but are also expected to advance to "autonomous self-healable". However, to integrate these features into flexible and stretchable devices, the first requirement to consider is compatibility between their mechanical and electrical properties given that the self-healing ability is associated with mechanical compliance but is incompatible with existing electronic technologies. Therefore, the first step closer to achieve is due to the recent progress in the field of stretchable semiconducting polymers, which thus far consists of two strategies: (1) structural engineering of conjugated polymers and (2) physical blending of conjugated polymers in soft insulating polymers. Together with the emphasis on additional functionalization in novel modified-semiconducting materials to boost large mechanical deformation without damaging their electronic properties, structural engineering can also provide targeted features (*i.e.*, self-healing ability). Finally, we highlight the chemical aspects of self-healing materials (from non-covalent to reversible covalent-based mechanisms) that have been successfully integrated in TFT devices.

Received 23rd May 2022,
Accepted 10th July 2022

DOI: 10.1039/d2ma00581f

rsc.li/materials-advances

1. Introduction

Since the discovery of polythiophenes and related conductive organic polymers by Heeger, MacDiarmid, and Shirakawa (Nobel Prize in Chemistry 2000),[1–3] numerous conjugated polymers have been developed as a new class of organic semiconductors, setting out to renew the semiconducting industry, which has been dominated by their inorganic counterparts such as traditional silicon-based materials over the last 50 years.[4] The fruit of this effort is reflected in the electronics revolution from heavy and cumbersome to compact and mobile and rigid

Department of Chemical Engineering, National Taiwan University of Science and Technology, No. 43, Sec. 4, Keelung Rd., Da'an Dist., Taipei City 10607, Taiwan. E-mail: ycchiu@mail.ntust.edu.tw

Livy Laysandra

Livy Laysandra received her MSc Degree from National Taiwan University of Science and Technology in 2020 under the guidance of Prof. Yu-Cheng Chiu. Currently, she is pursuing her doctoral degree at the same university. Her current research focuses on designing elastic and self-healing polymers as dielectric, semiconductor, and luminescent layers in thin-film form.

Andreas Njotoprajitno

Andreas Njotoprajitno joined Professor Yu-Cheng Chiu's lab at the Department of Chemical Engineering of National Taiwan University of Science and Technology (NTUST) in the spring of 2021 and achieved his BSc in the summer of 2022. His research focuses on the characterization of elastic and self-healing semiconducting polymers.

to flexible, and is expected to proceed to stretchable, ultimately changing the fundamental interactions between humans and technology. Thus far, striking progress has been achieved in various flexible electronic device applications such as soft robots,[5] e-skin sensors,[6–8] flexible devices,[9–12] wearable electronics,[13] and energy-storage devices.[14,15] However, these near-magnificence devices tend to fail in long-term use due to repeated wear and tear, accidental scratching, and mechanical fracture during deformation in their practical applications.[16] Consequently, researchers have sought to integrate healing capabilities to achieve a substantial improvement in device lifetime and increased reliability, maintainability, and durability.

However, the major challenge in the development of these polymers is maintaining good electrical and mechanical properties simultaneously. The extended π-conjugation of the polymer backbone is essential to yield good electronic properties, but the mechanical properties tend to be quite poor due to its high rigidity. Therefore, it is necessary to explore a much broader approach to fabricate semiconducting polymers having excellent mechanical properties without sacrificing their charge carrier mobility, especially for thin-film transistor (TFT) device application.

In this progress report, we comprehensively review the various approaches employed by different research groups to develop stretchable semiconducting polymers with emphasis on the design and manipulation of semiconducting polymers toward deformable stretchable electronics, a field which has grown significantly in the past few years.[17,18] We also provide an update on the current strategies developed toward intrinsically stretchable semiconducting materials as a starting point, among which two main strategies for diverse structural modifications have been adopted, as follows: (1) backbone engineering and (2) side-chain engineering, with each strategy having several unique approaches, as depicted in Fig. 1a. Then, highlighting the strong impact in the hydrogen bonding units incorporated in the conjugated polymer, intramolecular conformational locks can be established, resulting in increased backbone planarity, enhanced π-delocalization and field-effect mobility (μ_h^{FET}).[19–22] This elegant strategy also creates new properties and functions, one of which is self-healing ability (Fig. 1b).[23–25] The exceptionally successful building blocks that will be discussed in this review are exemplified by a range of different conjugated materials, including thiophene, diketopyrrolopyrrole (DPP), and isoindigo (IDG), containing polymers.[26–30] Furthermore, to outweigh the extra complexity introduced in modifying structural polymers, the simplicity of the physical blending of conjugated polymers in an elastomeric matrix for TFTs has been exploited (Fig. 1c).[31–33] Therefore, surveying the advances from extrinsically stretchable semiconducting polymer blends to self-healing capability is also necessary. We anticipate that the integration of these approaches will be crucial for the development of future-generation stretchable and self-healable polymer semiconductors.

2. Stretchable semiconducting polymers

Inspired by the overwhelming feature of elastomeric materials, many efforts have been devoted to replicating the mechanical properties of elastomers by integrating conjugated polymers in TFT applications to attain sufficiently high elasticity for stable

Suhendro Purbo Prakoso

Suhendro Purbo Prakoso received his PhD degree from Taiwan International Graduate Program on Sustainable Chemical Science & Technology (TIGP-SCST) in 2021 under the guidance of Prof. Chien-Lung Wang (Department of Applied Chemistry, National Yang Ming Chiao Tung University) and Prof. Yu-Tai Tao (Institute of Chemistry, Academia Sinica). Currently, he works as a postdoctoral fellow in Prof. Yu-Cheng Chiu's group. His current research interests involve the low-voltage, tunnelling-effect of photoassisted transistor memory devices and novel photosensitive charge storage materials.

Yu-Cheng Chiu

Yu-Cheng Chiu joined the Department of Chemical Engineering at National Taiwan University of Science and Technology (Taiwan Tech) as a tenure-track Assistant Professor since August 2017. Prior to joining the faculty, Yu-Cheng was a postdoc in the Zhenan Bao research group at Stanford University, where he was devoted to research on intrinsically stretchable/healable semiconducting polymers and high-performance OFET by solution shearing technique. Before moving to Stanford, he received his PhD degree under the supervision from Prof. Wen-Chang Chen in December 2012 from the Chem. E. at National Taiwan University, and then stayed in the same group for his first post-doctoral stint until 2014. Currently, his major interests are the elastic and self-healing semiconducting materials, soft organic devices including transistor and transistor memory, and morphology characterization for polymer materials.

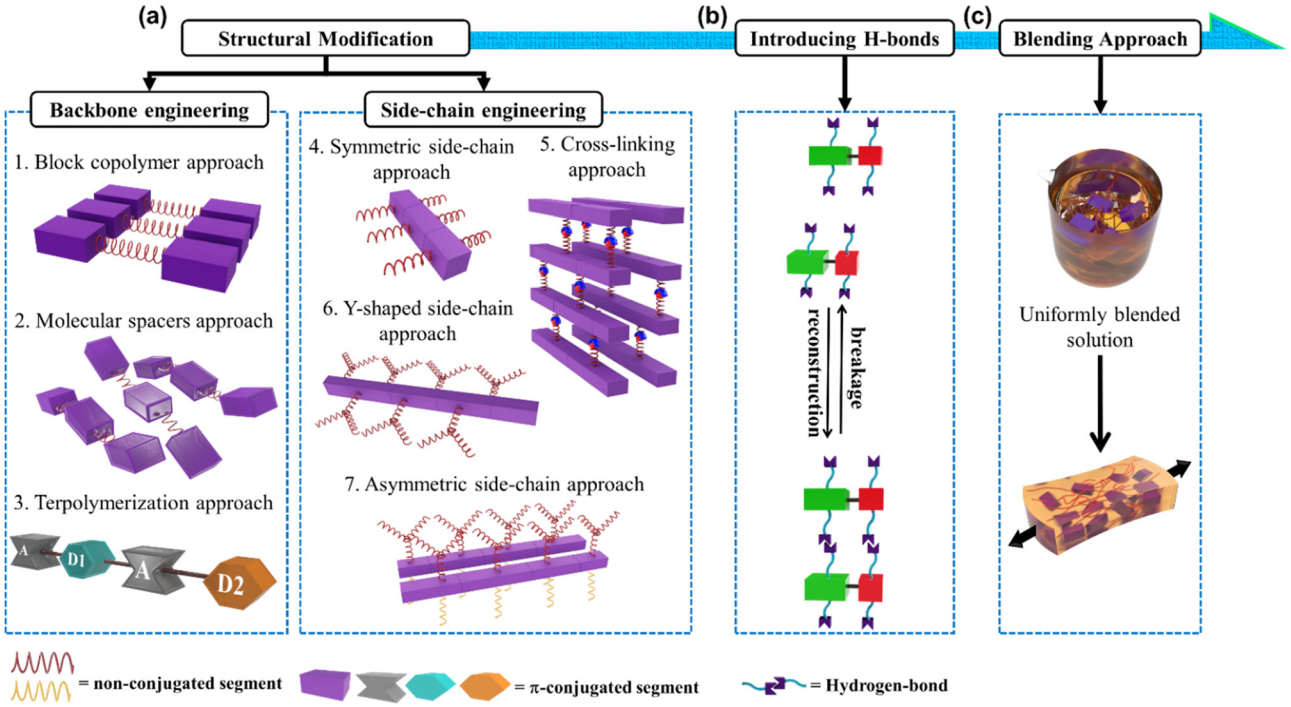

Fig. 1 Illustration of designing novel semiconducting materials to promote mechanical and electrical properties through: (a) structural engineering, which consists of two main strategies, and further divided into seven approaches; (b) functionalizing the side-chain using hydrogen bonding units; and (c) simple blending process of π-conjugated polymer with elastomer matrix, generating autonomous self-healing ability.

charge carrier transport under severe external stress.[34] Considering that the elastic properties of non-conjugated materials are influenced by the chemical nature of the monomer, branching, conformation, packing structure, extent of crosslinking, and chain length of macromolecules, exploitation of similar attributes in electrically active polymers bears great potential to achieve similar or even better mechanical properties.[35] The success of this approach can tremendously promote the potential of flexible devices, including the possibility of using low-cost fabrication methods over large-area substrates. In particular, Prof. Bao at Stanford University contributed greatly to the innovative development of this emerging field by utilizing the semiconducting polymer poly(3-hexylthiophene (P3HT)) to yield high-performance transistors.[36–40] Subsequently, flexible electronic devices began to develop rapidly. Several examples are presented and discussed in the next section, with emphasis on the details of the interrelation between the physical characteristics of the conjugated polymer structure with the mechanical-electronical compliance in TFT devices.

2.1 Fundamental properties of polythiophene derivatives

P3HT has emerged as a second-generation conjugated polymer that has successfully improved the performance of organic TFT devices.[4] Starting from the dedication of scientists to analyze and characterize the structural properties of P3HT, it was revealed that one of the most compelling properties of P3HT is its ability to form highly ordered π-stacks and side-chain lamella stacks.[39,41,42] Transmission electron microscopy (TEM) has been used to demonstrate the structural evolution from chain-extended crystals to an architecture consisting of interlinked crystalline lamellae and amorphous regions at a weight-average molecular weight (M_w) of around 25–35 kg mol^{-1}.[41,42] Furthermore, the long-range packing behavior and morphology of a P3HT film was observed *via* atomic force microscopy (AFM), providing information about its assembly mechanism and the aligning effects of various deposition methods. Obviously, chain folding, which leads to lamellar crystalline units, was discovered in classical systems such as polyolefins and poly(ethylene oxides)[43–45] and visualized in longer-chain P3HT molecules by scanning tunnelling microscopy (STM) in early 2000 by Mena-Osteriz *et al.*[46] In brief, the well-controlled M_w P3HT chains can fold and may possess sufficient connections (or tie chains) between ordered domains, resulting in higher charge mobility compared with low-M_w P3HT.

Focusing on the typical semicrystalline P3HT morphology composed of anisotropic crystalline regions bridged by tie chains (Fig. 2a),[47,48] the possibility of intrinsic stretchability can be expected. As the first step in investigating the strong correlation between the strain-alignment and charge mobility of P3HT thin films, O'Connor *et al.* proposed an innovative strategy to align the crystalline phase in P3HT, which was achieved by laminating a P3HT spin-coated film on a stretchable poly(dimethylsiloxane) (PDMS) substrate, and then stretching to various extents.[49] Upon stretching, the crystallites in the P3HT films were reoriented with the polymer backbones aligned in the direction of the applied strain. The mobility of P3HT increased in the applied strain direction and decreased in the perpendicular direction. This strain-induced alignment

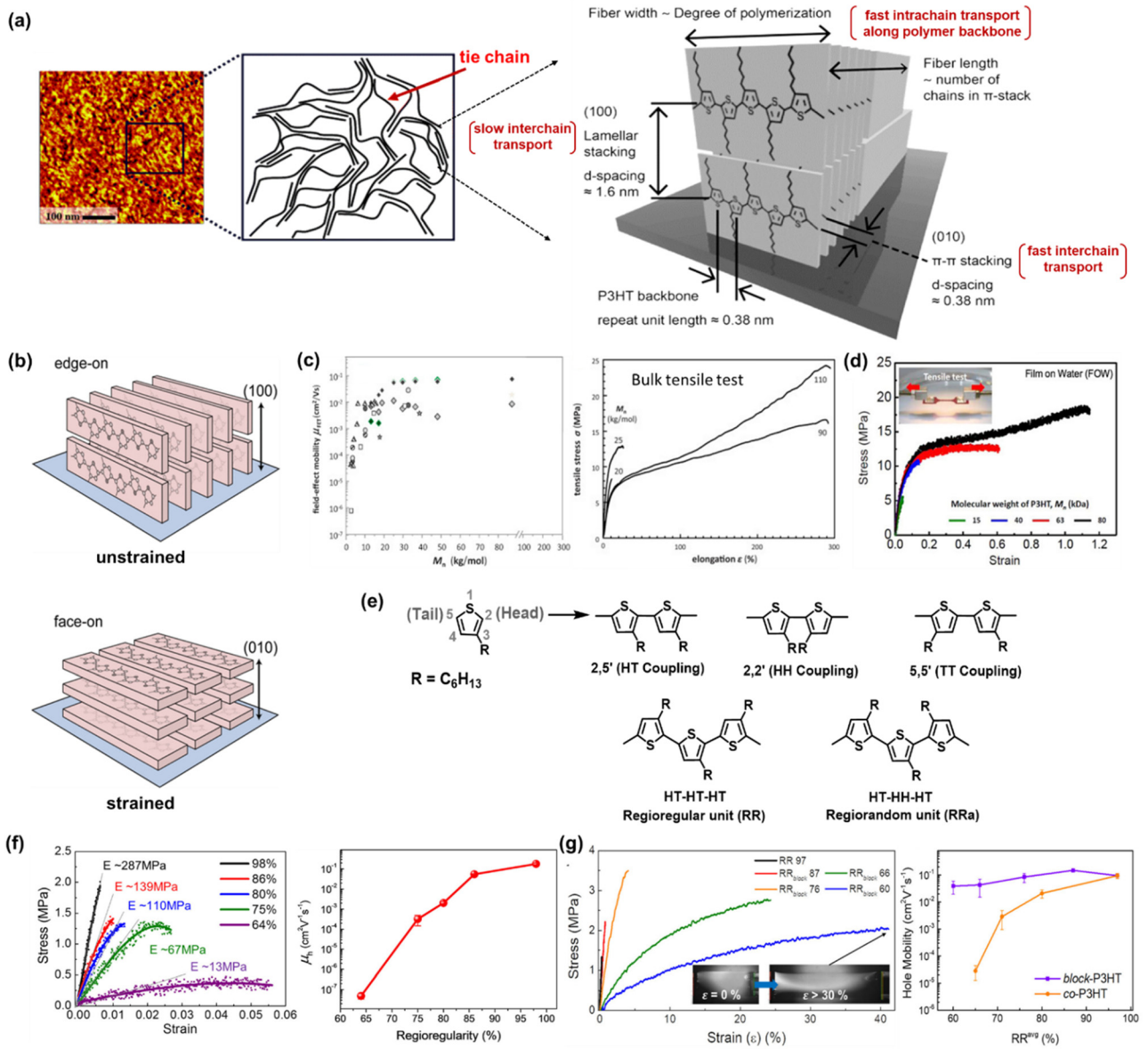

Fig. 2 Structure engineering of polythiophene derivatives. (a) Atomic force microscopy (AFM) image of P3HT film (left), schematic of molecular structure consisting of anisotropic crystalline region bridged by amorphous regions (middle), and crystallographic molecular structures of the semicrystalline P3HT packing behavior showing directions of π-stacking and lamellar-stacking (right). (left and middle)[47] Copyright: 2005, the American Chemical Society. (right)[48] Copyright: 2017, the American Chemical Society. (b) Illustration of the P3HT backbone stacking orientation before and after strain. The polymer crystallites reorient to align in the direction of the applied strain, transforming the edge-on crystallites into face-on crystallites.[50] Copyright: 2013, the American Chemical Society. (c) Hole mobilities and stress–strain curves of P3HT tapes as a function of M_n.[52] Copyright: 2013, Elsevier. (d) stress–strain curves and tensile moduli of P3HT thin films at different M_n obtained by film-on-water (FOW) technique.[53] Copyright 2017, the American Chemical Society. (e) Schematic showing three possible coupling modes and chemical structure of regioregularity (RRe) and regiorandom (RRa) of P3HT. (f) stress–strain curves and hole mobilities of P3HT films with respect to the degree of regioregularity M_n obtained by the FOW technique.[58] Copyright: 2015, the American Chemical Society. (g) Schematic illustration of *block*-P3HTs with increasing lengths of RRa-blocks added for mechanically robust and high-performance TFTs, the stress–strain curves of *block*-P3HTs (the inserted picture of the RR_{block} 60 film shows that no damage occurred even after stretching above 30% strain), and hole mobility values as a function of RRe-*block*-P3HTs.[59] Copyright: 2019, the American Chemical Society.

transformed the predominant edge-on oriented (100) polymer crystallites to face-on orientation (010) crystallites (Fig. 2b). Alternatively, 100% biaxially stretched films showed an increase in facial alignment, but the charge mobility anisotropy was not significant.[50] These results suggest that mechanical strain on the micrometer scale can produce changes in texture, anisotropy in elastic modulus, and alter charge transport. Furthermore, molecular engineering seeks to attain the integration of different features by focusing on the structure–property relationship at the molecular level such as molecular weight (M_w), regioregularity (RRe), and other considerations related to solution processing and fabrication techniques. In the following section, we specifically

discuss the influence of these crucial parameters on charge transport and mechanical properties.

2.1.1 Molecular weight effect. Together with molecular structure design, molecular weight and dispersity have been well documented as unavoidable-parameters that exert a significant impact on most of the physical properties of polymers.[51] The charge carrier mobility in P3HT is the same. Koch *et al.* reported that the μ_h^{FET} in P3HT increased by several orders of magnitude (from 10^{-5} to 10^{-1} cm^2 V^{-1} s^{-1}) in a relatively narrow range of molecular weights (2–25 kg mol^{-1}) with PDI between 1.0–2.0, and then became saturated (Fig. 2c).[52] Meanwhile, by subjecting melt-processed P3HT tapes of various number-average molecular weights (M_n = 20, 25, 90 and 110 kg mol^{-1}) to a mechanical tensile test, the low M_n P3HT displayed brittle tensile behavior, rupturing below 10% strain and higher elastic modulus. A high M_n showed plastic deformation, exhibiting very high extensibilities (nearly 300%) prior to fracture with the greatest mechanical strength of 24 MPa. This phenomenon represents the softening effect of MW in P3HT and related to the structural organization. A similar trend was assayed in thin film immersed in water by Rodriquez *et al.* (Fig. 2d).[53] In this case, the ductility (strain at fracture) and toughness (total energy density absorbed by the material at the point of fracture) increased with an increase in molecular weight, but became saturated at approximately 40 kDa, while the maximum extensibility continued to increase to more than 100% for 80 kDa as the highest molecular weight tested. Microstructurally, it has been proven that semiconducting polymers with high M_n bear greater resilience to cracking as a result of their higher chain entanglement, lower crystallinity, and tie chain bridging stress across crystallites. In contrast, a low M_n is associated with the presence of highly ordered needle-like aggregates, which in principle can stiffen the films. Definitely, it is favorable to maximize the M_n of conjugated polymers up to a certain point for achieving superior mechanical and electric properties.

2.1.2 Regioregularity effect. P3HT exhibits three possible orientations when two thiophene rings are coupled (*i.e.*, head-to-head (HH), head-to-tail (HT), and tail-to-tail (TT)) (Fig. 2e). P3HT with mainly the HT orientation ($\geq$95%) is referred to as a regioregular (RRe) structure, leading to ordered interchain packing. In contrast, other configurations such as HH and TT coupling lead to distributed chain conformations of the regiorandom (RRa) P3HT owing to the steric hindrance between the nearest hexyl side chains. Early studies reported that RRe P3HT resulted in higher crystallinity and higher charge mobility compared to RRa isomers.[36,39,54–57] As an example, Sirringhaus *et al.* revealed that 96% RRe P3HT possessed a high carrier mobility of up to 10^{-1} cm^2 V^{-1} s^{-1}, whereas less RRe P3HT ($\sim$80%) exhibited low mobilities of about 2×10^{-4} cm^2 V^{-1} s^{-1}.[56,57] Since the regioregularity (RRe) of a polymer can control the crystallinity of thin films, it may also influence their mechanical properties. Kim *et al.* reported that the mechanical and electrical properties of P3HT could be effectively controlled by tuning the degree of RRe.[58] P3HT was synthesized *via* Grignard metathesis (GRIM) polymerization, which allows excellent control of the RRe degree with a comparable M_n and low PDI. It should be noted that the authors employed a film-on-water (FOW) technique to validate the intrinsic mechanical measurements. As shown in Fig. 2f, the elongation at break value of P3HT was significantly improved from 0.6% to 5.3% with respect to a reduction in the degree of RRe from 98% to 64% (RRe-98 to RRe-64). Conversely, the tensile moduli tended to decrease from 287 MPa to 13 MPa, given that the amorphous regions in low RRe P3HT films disrupt their crystalline packing behavior. Meanwhile, the highly crystalline RRe-98 P3HT polymer provided a great average μ_h^{FET} of 0.18 cm^2 V^{-1} s^{-1}, while the average μ_h^{FET} of RRe-64 was only 4.8×10^{-8} cm^2 V^{-1} s^{-1}. Thus, the high RRe P3HT showed strong crystallinity, leading to high charge carrier mobility but suffered from severe mechanical failure. By contrast, regiorandom (RRa) P3HT films can sustain large mechanical deformations without failure; however, it usually leads to a decrease in their electrical performance.

Considering the disadvantages of using a homopolymer with randomly coupled HH defects, in the case with a limited extent of ordered domains, the same research team continued the development of mechanically robust and high-performance TFT using a P3HT regioblock copolymerization strategy (*block*-P3HTs).[59] The authors prepared a series of *block*-P3HTs consisting of RRe and RRa P3HTs with various M_n values of RRa blocks (from 3 to 33 kg mol^{-1}) and a fixed M_n of RRe blocks (11–12 kg mol^{-1}) *via* a catalyst-transfer polycondensation strategy (Fig. 2g). Briefly, *block*-P3HT thin films with longer RRa blocks enhanced the mechanical ductility due to the fact that the amorphous moiety in regioblock copolymers promotes the formation of an entangled and/or folded structure. For example, the elongation at break of the thin films was remarkably enhanced by 100-fold (*i.e.*, from 0.3% to 30.2%) as the M_n of the RRa block increased. Amazingly, all the *block*-P3HT possessed a similar high μ_h^{FET} of 1.5×10^{-1} cm^2 V^{-1} s^{-1} to that of the high RRe P3HT homopolymer. The discovery of the mechanical ductility of *block*-P3HTs, which can be dramatically enhanced without sacrificing the electrical properties, becomes ones of the promising candidate strategies to fabricate high-performance soft electronics, considering the trade-off between electronic properties and mechanical flexibility often encountered by scientists.

2.1.3 Solution processing and fabrication effect. The mobility together with the deformability of polymer packing by altering the film preparation or processing conditions, such as annealing temperature and solvent choice, have also been considered.[36,60–65] These considerations are based on the relationship between the film morphology and mechanical compliance by M_n and regioregularity effects. An early study by Bao *et al.* reported both high carrier mobilities (*i.e.* 4.5×10^{-2} cm^2 V^{-1} s^{-1} in the accumulation mode and 1×10^{-2} cm^2 V^{-1} s^{-1} in the depletion mode) and on/off current ratios close to 10^4 for their RRe P3HT ($\geq$95%) using solution casting.[36] The mobility of RRe P3HT was found to vary by two orders of magnitude depending on the choice of solvent used. This investigation confirmed that the mobility of RRe P3HT varied greatly with the solvent employed for its fabrication. The

effect of annealing polymers was demonstrated by O'Connor *et al.*, where the annealed poly-(2,5-bis(3alkylthiophene-2-yl)-thieno[3,2-*b*]thiophene) (PBTTT) exhibited an increase in elastic modulus from 0.9 to 1.8 GPa, where the increase in modulus upon annealing is consistent with the increase in crystallinity, resulting in an enhancement in charge transport.[60] Moreover, polymer packings are comprised of different levels of aggregates, evaporation rates, and nanofibril formation tendencies, which are influenced by the annealing temperature and choice of solvent.[66–70]

In the preparation of polymers, it is necessary to consider parameters such as the film preparation method (ultrasonication, spin-coating, dip-coating, drop-casting, melt processing, and blade coating) given that they can influence their morphology, regioregularity, and change in M_n in comparison to conjugated polymers, which are structurally different, to fairly assess their structural contribution.[38,71,72] Another example by Choi *et al.* showed that ultrasonication led to the formation of P3HT nanowires with increased mobility, film crystallinity, and decreased crack onset strains.[73] Therefore, ultrasonication plays an important role in breaking down the polymer chain, enhancement in aggregation, and local order for inter-and intramolecular interactions. The mechanical behavior could be observed in the tensile test of melt-processed P3HT and spin-coated P3HT, as shown in Fig. 2c and d, respectively. The optimal maximum strain value of the melt-processed high M_n P3HT reached 300%, whereas the spin-coated film was only stretchable up to 100%. The variation in film thickness and its morphology may also cause a significant difference in critical strain.

2.2 Conjugated polymer engineering

Another notable aspect to promote the mechanical deformability and charge-transporting capability of stretchable semiconductor polymers arises from the diverse structural modification of conjugated polymers. This type of approach was highlighted by the finding of O'Connor *et al.* when comparing RRe P3HT and PBTTT.[60] The correlation between μ_h^{FET} and elastic moduli was displayed with moderately crystalline P3HT and highly crystalline PBTTT, exhibiting low and high μ_h^{FET}, respectively, while their elastic moduli showed a proportional trend with μ_h^{FET}. As has been discussed previously (see Fig. 2a), P3HT adopts an edge-on type lamellar packing motif of polymer backbones bridged by alkyl chain regions. The π-stacking direction in a parallel way to the substrate enables efficient 2D charge transport favorable for TFTs. In contrast, PBTTT more easily forms highly ordered films due to the existence of many crystalline domains with larger crystalline sizes and fewer defects. This superiority in terms of μ_h^{FET} (8×10^{-2} cm^2 V^{-1} s^{-1}) and elastic modulus (E = 0.9 GPa) of PBTTT over P3HT (μ_h^{FET} = 6×10^{-2} cm^2 V^{-1} s^{-1} and E = 0.25 GPa) is due to its higher crystalline morphology. Furthermore, the high crystallinity is also responsible for the low crack onset strain for PBTTT (<2.5%) compared to P3HT (>150%). These results illustrate that long-range order is preferable to increase the mobility, but inevitably stiffens and embrittles the polythiophene semiconductor films.

Considering the high crystallinity and amorphous nature of conjugated polymers, it is assumed that their electrical-mechanical properties are mutually exclusive. However, through the continuous efforts and exploration by researchers, it was discovered that conjugated polymers based on isoindigo (IDG), naphthalene diimides (NDI), and diketopyrrolopyrrole (DPP)[26–30] exhibit impressive charge mobilities of over 1 cm^2 V^{-1} s^{-1} although their long-range order is relatively poorer than that of P3HT and PBTTT. These observations have led to a new way of generating conjugated polymer thin films for effective charge mobility, thus facilitating the optimum intra- and intermolecular charge transport at the device length scale, improving the interconnectedness between aggregated domains, and reducing the amount of disorder in the conjugated segments (making rigid backbones) seem to be the key rather than inducing high crystallinity.[74–76] Hence, two main strategies of diverse structural modifications have been adopted, *i.e.*, backbone engineering and side-chain engineering (Fig. 1a). Backbone engineering involves the introduction of conjugated and non-conjugated units into the main chain of a polymer, which is generally classified into three approaches, mainly block copolymerization, molecular spacer, and terpolymerization. Meanwhile, side chain engineering introduces non-conjugated units in the side chain of a conjugated polymer, which can also be classified into four different approaches, including symmetric/asymmetric side-chain, cross-linking, and Y-shaped side-chain. Furthermore, it was revealed that the incorporation of hydrogen bonding moieties in these novel conjugated polymer designs is particularly effective in tailoring the mechanical deformability and maintaining or even boosting the charge transport values in TFTs.[19–22] Interestingly, the combination of dynamic H-bonds in organic semiconductors has created new properties and functions such as self-healing ability which will be explained in Section 3.[23–25]

2.2.1 Block copolymer approach. Attaching soft and insulating segments in the conjugated backbone is a widely used approach to develop a new class of intrinsically stretchable semiconducting multiblock copolymers because the presence of a flexible insulating segment reduces the glass transition temperature (T_g) of polymers and decreases the π–π stacking and crystallinity of polymer semiconductors in the solid-state. Müller *et al.* (2007) designed semiconducting diblock copolymers containing various weight ratios of P3HT as the rigid segment and polyethylene (PE) as the soft segment (Fig. 3a).[77] The rigid P3HT homopolymer featured a high Young's modulus of up to 28 MPa and elongation at break of only 13%. However, by incorporating soft PE blocks with a content as high as 65 wt%, the diblock copolymer showed an impressive Young's modulus of 240 MPa and maximum elongation of over 600% before break. Interestingly, the 35–65 wt% P3HT-PE possessed a decent μ_h^{FET} of 5×10^{-2} cm^2 V^{-1} s^{-1}, which is comparable to the maximum FET-mobility values reported for non-stretchable P3HT homopolymer.[36,78] Thus, P3HT-PE displays very useful semiconductor properties even at a low P3HT content. Subsequently, the success of this strategy prompted the curiosity of researchers to combine P3HT with other soft-type materials. Chen and Satoh group investigated the influence of low-T_g

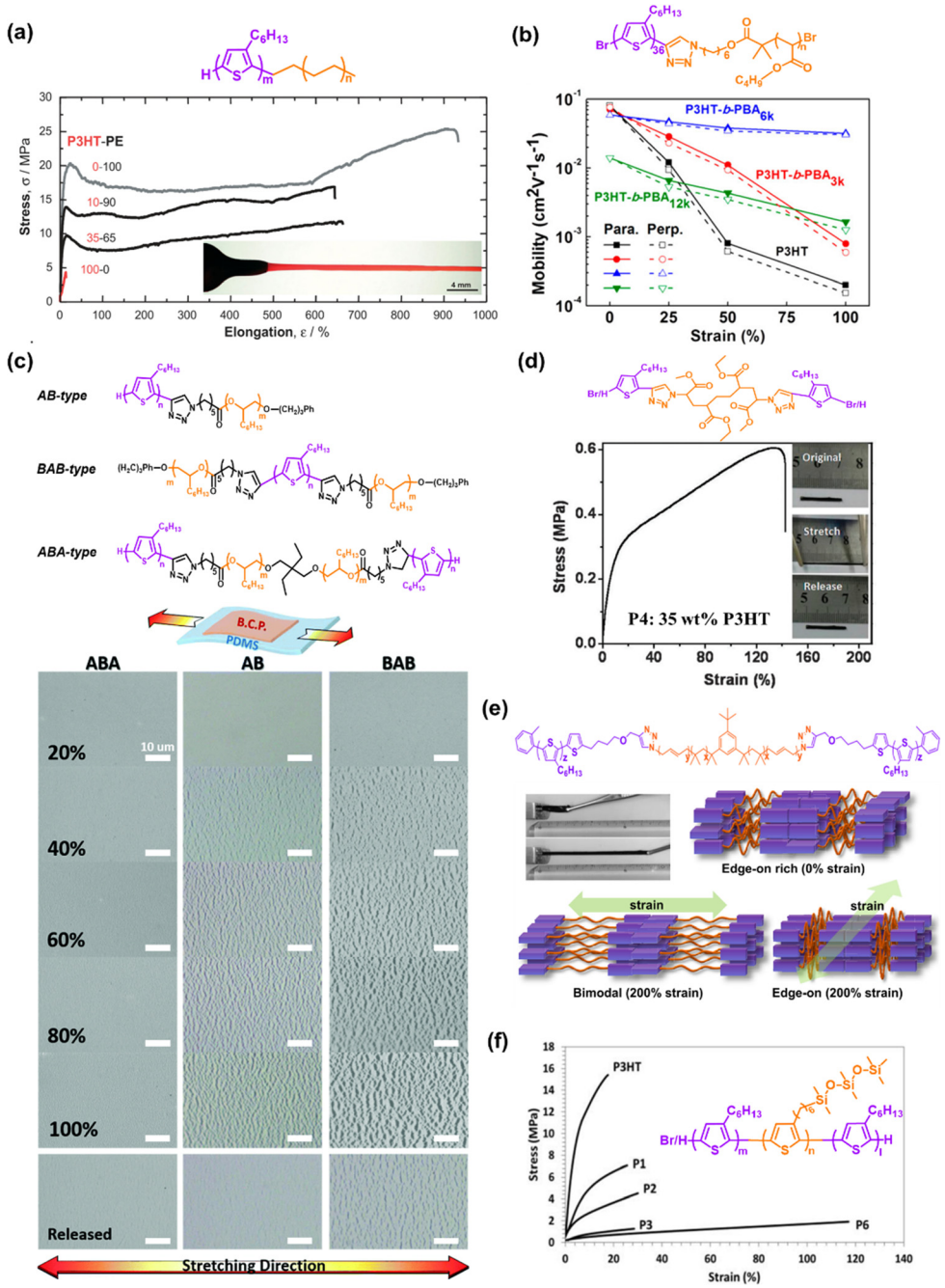

Fig. 3 Intrinsically stretchable semiconducting polymers developed based on the block copolymer approach. The chemical structures and mechanical and/or electrical properties of: (a) diblock copolymers with different weight ratios of P3HT and PE. The inset of the bottom image is an optical image of a dog-bone-shaped 35–65 wt% P3HT-PE under 600% stretching.[77] Copyright: 2007, Wiley-VCH. (b) P3HT-*b*-PBA rod-coil diblock copolymers.[79] Copyright: 2017, the American Chemical Society. (c) AB-type, BAB-type, and ABA-type of P3HT-*b*-POO block copolymers.[80] Copyright: 2019, The Royal Society of Chemistry. (d) Triblock copolymer P3HT-*b*-PMA-*b*-P3HT.[81] Copyright: 2015, The Royal Society of Chemistry. (e) P3HT-*b*-PIB-*b*-P3HT with a photograph of the triblock copolymer film before and after stretching (upper left) and illustration of the model for the deformation of the microphase separated structure and crystalline orientation of the triblock copolymer thin film (bottom).[82] Copyright: 2015, the American Chemical Society. (f) P3HT-*b*-P3SiHT-*b*-P3HT, where the stress–strain profile composed of the homopolymer P3HT (Mn = 20 kg mol^{-1}), diblock copolymer P3HT-*b*-P3SiHT (P1–P3 where PI, P2, and P3 containing 73, 60, and 53 wt% P3HT, respectively), and triblock copolymer P3HT-*b*-P3SiHT-*b*-P3HT containing 22 wt% P3HT (P6).[83] Copyright: 2018, Wiley-VCH.

poly(*n*butyl acrylate) (PBA) segments in the rod-coil diblock copolymers (P3HT-*b*-PBA).[79] As expected, the tensile modulus of the P3HT-*b*-PBA thin films decreased from 0.63 GPa (P3HT-*b*-PBA_{3k}) to 0.19 GPa (P3HT-*b*-PBA_{12k}) with an increase in the block length of PBA (Fig. 3b). Even after 100% mechanical strain, P3HT-*b*-PBA_{6k} displayed a high μ_h^{FET} of 2.5×10^{-2} cm^2 V^{-1} s^{-1} with

an on/off ratio of 7.2×10^6, and it could still maintain its mobility at the same magnitude after further stretching-releasing up to 1000 cycles. This result indicates that an optimized block ratio (P3HT-*b*-PBA_{6k}) can provide promising stability and reproducibility. In addition, the same group expanded on this work by using poly(octylene oxide) (POO) as the soft segment with different molecular architectures (AB-, ABA-, and BAB-type block copolymers), where A is the P3HT block and B is POO block.[80] Among the conjugated-elastic block copolymers, only the ABA-type block copolymer thin film remained perfectly smooth and no cracks were observed even up to 100% strain (Fig. 3c). Meanwhile, the average hole mobilities of the ABA-type, AB-type, and BAB-type block copolymer-based field-effect transistors were 2.5×10^{-4}, 1.2×10^{-4}, and 7.5×10^{-5} $cm^2 V^{-1} s^{-1}$, respectively, which may be caused by the sizes of the crystalline nanofibrils. The larger and longer nanofibrils offer more appealing charge-transfer mobilities.

As another example of more advanced molecular backbone engineering, Peng *et al.* (2015) first proposed the concept of utilizing hard-soft-hard (ABA-type) triblock copolymers based on the principle of architectural thermoplastic elastomers (TPEs), leading to the formation of intrinsically stretchable semiconductor TPEs (Fig. 3d).[81] The authors succeeded in synthesizing ABA triblock copolymers consisting of crystalline P3HT as A and amorphous polymethacrylate (PMA) block as B. The novel ABA triblock copolymer demonstrated a high Young's modulus of 6 MPa, stretchability of 140%, and μ_h^{FET} of 1.7×10^{-4} $cm^2 V^{-1} s^{-1}$ despite containing 65 wt% PMA. Inspired by the semiconductor TPE design, Higashihara *et al.* (2019) used a similar approach to prepare a novel intrinsically stretchable ABA-type triblock copolymer composed of P3HT and polyisobutylene (PIB) segments (P3HT-*b*-PIB-*b*-P3HT) (Fig. 3e). Due to the excellent elastomeric properties of the PIB segments,[82] this polymer exhibited an extremely low elastic modulus of 0.00113 GPa and a much improved crack onset strain value of 300%, as determined *via* the tensile test in bulk films, with the μ_h^{FET} value of 3.0×10^{-3} $cm^2 V^{-1} s^{-1}$ despite containing 70 wt% insulating PIB. Given the fact that these polymers possessed insulating and non-semiconducting segments, it is not surprising that the mobility of the triblock copolymers decreased as the soft-material content increased.

Recognizing this weakness, Miyane *et al.* (2018) fabricated fully conjugated ABA triblock polymers by utilizing a regioregular polythiophene derivative bearing a trisiloxane group in the side chains (P3SiHT) as the soft segment.[83] The merits of the introduction the P3SiHT moiety in conjugated polymers have been further investigated.[84–87] Indeed, a P3SiHT film displayed a remarkable change in characteristics such as thermal behavior, chemical stability, mechanical property, and miscibility in solvents. Especially in terms of mechanical behavior, it exhibited 2-orders of magnitude smaller Young's modulus and 20 times higher elongation at break than RRe P3HT.[87] Benefiting from the features of P3SiHT, all the block copolymers exhibited a lower tensile modulus and greater elongation as the P3SiHT content increased, which are typical characteristics of a plastic-to-rubber transition. As illustrated in Fig. 3f, P3HT-*b*-P3SiHT-*b*-P3HT with the highest P3SiHT content of 78 wt% delivered a low elastic modulus of 0.00335 GPa and improved elongation at break of 118%. Interestingly, the resulting μ_h of the ABA triblock copolymer in the TFTs were unexpectedly comparable or even higher than that of the P3HT homopolymer. P3HT-*b*-P3SiHT-*b*-P3HT with the lowest P3HT content of 22% exhibited an even higher average mobility (5.14×10^{-3} $cm^2 V^{-1} s^{-1}$) than the P3HT homopolymer (1.46×10^{-3} $cm^2 V^{-1} s^{-1}$). Among the prepared copolymers, P3HT-*b*-P3SiHT-*b*-P3HT with 59 wt% P3HT obtained an excellent average μ_h^{FET} value of 1.06×10^{-2} $cm^2 V^{-1} s^{-1}$. Overall, by leveraging its ability to assemble well-defined structures on the nanoscale, the block copolymer approach plays an important role in efficiently optimizing the mechanical properties of materials. This approach offers a way to avoid complex structural engineering for the fabrication of devices, but the development of stretchable materials suitable for electronic devices is a great challenge. Thus far, the low μ_h^{FET} with P3HT-based modification still cannot satisfy the theoretical intrinsic intracrystalline mobility of RRe P3HT, which can reach over 1 $cm^2 V^{-1} s^{-1}$.[88–90] Thus, it seems that the block copolymer approach still needs to be further developed to actualize the application of high-performance devices in terms of both electrical-mechanical properties.

2.2.2 Molecular spacer approach. As reported by Müller's group, in P3HT-*b*-PE, it is possible for a conjugated polymer to retain favorable charge-transport properties despite the fact that most diblock copolymers are composed of insulating segments.[77] In contrast to the modification of the polymer without interfering with its conjugated units, Mei and co-workers used diketopyrrolopyrrole (DPP) donor–acceptor (D–A) polymers to improve the ductility and reduce the modulus, and simultaneously retain much of their electronic performance, while interrupting the rigid conjugated backbones with flexible 1,3-propylene (C3) spacer units.[26] It was revealed that the DPP-20 mol% conjugation break spacer (CBS) unexpectedly maintained relatively high charge mobility of over 1.0 $cm^2 V^{-1} s^{-1}$, which is insignificantly different from an average mobility of DPP-0 mol% CBS (4.3 $cm^2 V^{-1} s^{-1}$). The same research group collaborated with Thompson's group, introducing a concept of CBS in the polymer backbone to reduce the crystallinity and T_g, which consequently impart stretchability.[91,92] In these reports, a series of semi-random polymers with varying spacer lengths and spacer compositions were examined (Fig. 4a).[92] Consequently, the 10% T-10-T polymer sample exhibited relatively high hole mobility based on its space charge-limited current (SCLC) (μ_h^{SCLC}) value of 2.53×10^{-4} $cm^2 V^{-1} s^{-1}$, which was comparable to that of its fully conjugated counterpart (P3HT-DPP-10%) of 9.29×10^{-4} $cm^2 V^{-1} s^{-1}$. Interestingly, although the hole mobility decreased with an increase in spacer composition, there is still an increment in hole mobility with respect to the length of the spacer carbon chain. Through the film-on-elastomer measurement, it was revealed that several modified polymers could be stretched beyond 80% strain, and particularly for 10% T-8-T and 10% T-10-T, they could achieve the lowest elastic modulus of 0.14 GPa and 0.15 GPa, respectively. This approach

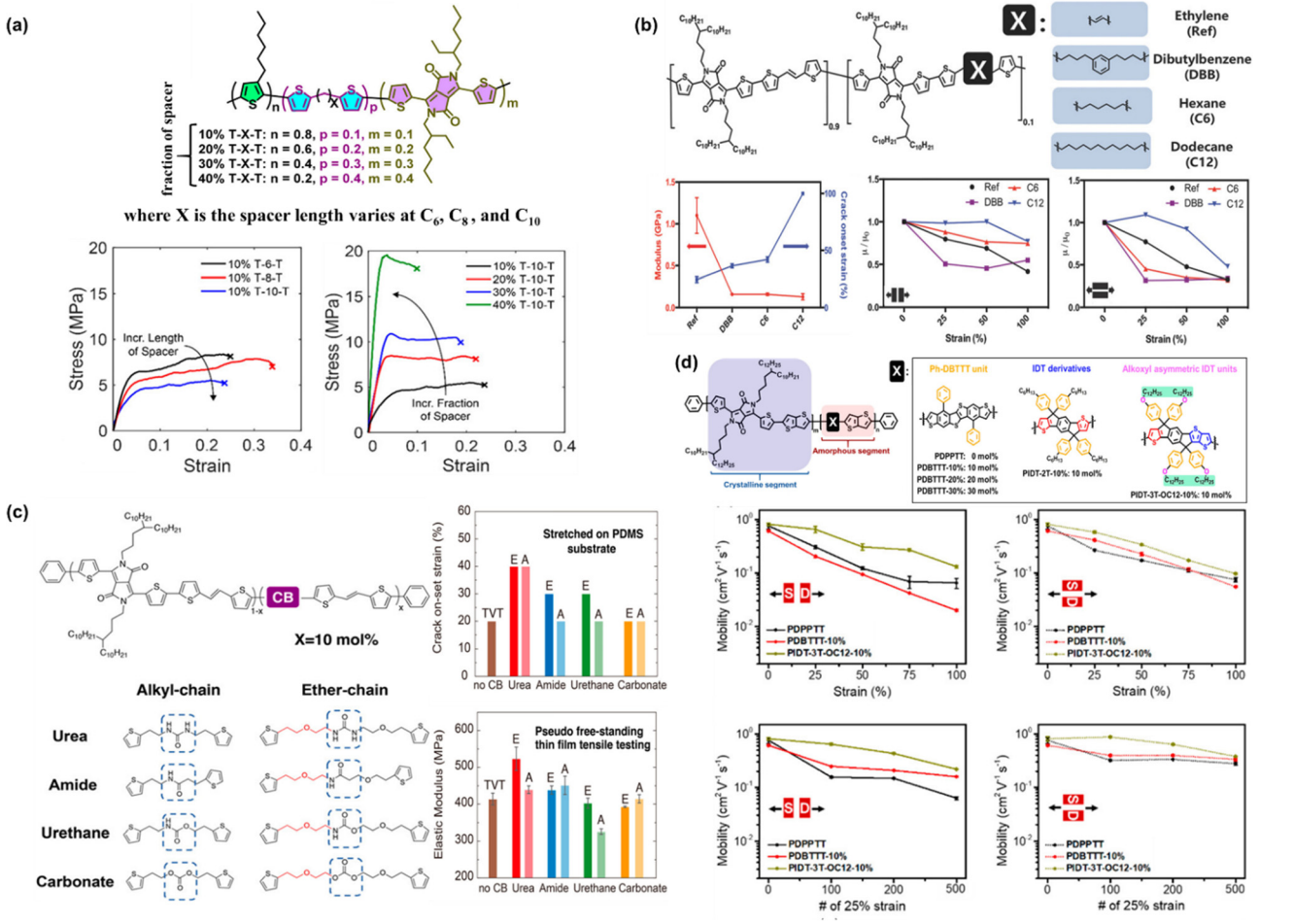

Fig. 4 (a) Chemical structure of the designed DPP-based conjugated polymer backbone and the effect of the conjugation-break spacer length and spacer composition on its mechanical and electrical properties. Representative stress–strain curves of modified P3HT-DPP polymer films obtained using the FOW technique.[92] Copyright: 2018, the American Chemical Society. (b) Effects of chain breakers on elastic modulus and mobility under strain in DPP-TVT polymers.[93] Copyright: 2018, Wiley-VCH. (c) Summary of the crack on-set and elastic modulus measurements of DPP-TVT polymers as a function of the H-bonding conjugation breaker effect.[94] Copyright: 2020, the American Chemical Society. (d) Effect of conjugated rigid fused-rings with optimized bulky side groups in the conjugated polymer backbone.[95] Copyright: 2021, the American Chemical Society.

opens an avenue for researchers to overcome the most common obstacle of the tradeoff between mechanical and electronic performance.

Mun *et al.* investigated the influence of flexible conjugation breakers in the DPP/thienylene vinylene (TVT) polymer semiconductor backbone, in which three different chain breakers were used, *i.e.*, ethylene, dibutylbenzene (DBB), hexane (C6), and dodecane (C12).[93] Upon the incorporation of 10% molar ratio chain breaker, the non-conjugated segments could "tune" the mechanical properties, while maintaining high mobility of higher than 1 $cm^2 V^{-1} s^{-1}$, as shown in Fig. 4b. Remarkably, the C12-DPP/TVT polymer thin films exhibited a largely improved crack onset strain as high as 100% strain and a low modulus of 0.13 GPa, which could maintain moderate mobility (>0.36 $cm^2 V^{-1} s^{-1}$) under 100% strain even after a hundred cycles of 50% strain. Compared to DPP/TVT-based polymer films containing other conjugation breakers, C12-DPP/TVT was revealed to exhibit the best balanced performance in terms of both mechanical and electrical properties. Moreover, the effect of the three chain breakers on all the polymer derivatives was still more ductile with a lower elastic modulus compared to the reference polymer using ethylene as the chain breaker. It should be noted that the obtained higher stretchability of the C12-DPP/TVT thin films originates from their lower crystallinity, as confirmed by T_g measurements and X-ray diffraction. To further understand the effects of the H-bonding strength, Zheng *et al.* studied its influence on the mechanical and electrical properties of polymer semiconductor thin films using different types of H-bonding units (urea > amide > urethane > carbonate) and linker flexibilities (ether chain (E) > alkyl chain (A)) (Fig. 4c).[94] Basically, H-bonding units were incorporated as CBS into a DPP D–A conjugated polymer backbone. It was observed that E-urea and A-urea with stronger H-bonding (self-association constant of >0.7) and flexible linkers having a higher tendency for denser packing could induce higher polymer chain aggregation and crystallinity in thin films, resulting in an improvement in the modulus and crack on-set strain and less degradation in mobility during stretching. It has to be

emphasized that the E-urea/E-amide-derived polymers exhibited the highest charge transport mobilities due to their high crystallinity and intense H-bonding.

The same concept is applicable to other material systems, another example of which is the introduction two distinct classes of rigid fused-ring systems in a poly(thieno[3,2-*b*]thiophene-diketopyrrolopyrrole) (PDPPTT) backbone. The rigid fused-ring systems investigated by researchers, namely, benzene-substituted dibenzothiopheno[6,5-*b*:6′,5′-*f*]thieno[3,2-*b*]thiophene (Ph-DBTTT) and indacenodithiophene (IDT) systems.[95] In fully stretchable transistors, as shown in Fig. 4d, the PIDT-3T-OC12-10% polymer showed a mobility of 0.27 $cm^2 V^{-1} s^{-1}$ at 75% strain and maintained its mobility after being subjected to hundreds of stretching-releasing cycles at 25% strain. Compared to the reference polymer PDPPTT, the device showed an abrupt drop in mobility when stretched either parallel to the strain direction (∥) or perpendicular to the strain direction (⊥) from 0% to 75% strain, in which the initial mobility of 0.76 $cm^2 V^{-1} s^{-1}$ decreased to $\mu_{h\parallel}^{FET} = 7 \times 10^{-2}$ $cm^2 V^{-1} s^{-1}$ and $\mu_{h\perp}^{FET} = 1.1 \times 10^{-2}$ $cm^2 V^{-1} s^{-1}$ at 75% strain. After 500 cycles at 25% strain, the tested devices all showed a low $\mu_{h\parallel}^{FET} = 6 \times 10^{-2}$ $cm^2 V^{-1} s^{-1}$ in the parallel stretching direction due to crack formation at 25% strain. These results underscore the intimate correlation between chemical structures, mechanical properties, and charge carrier mobility of polymer semiconductors.

2.2.3 Terpolymerization approach. Many previous studies revealed that the CBS approach can lower the backbone rigidity and revamp the stretchability of polymer semiconductors, despite the uncertainty in their electrical performance. Thus, to alleviate this issue, engineering conjugated monomer structures that are more complex than the binary system of conventional D–A copolymers has been pursued to enhance the stretchability without compromising charge transport.[96–100] The most prominent example is conjugated random terpolymers, including A–D–A′–D- and/or A–D–A–D′-type copolymers. It was revealed that these conjugated random terpolymers can be used to effectively fine-tune the crystallinity and aggregation behaviors of the reference parent polymers. Owing to the mismatched geometry induced by additional components, random ternary copolymers are expected to possess reduced crystallinity compared to their reference parent polymers. Lin *et al.* utilized an elegant strategy to randomly incorporated different amounts of isoindigo (IID) unit in the reference DPP-quaterthiophene conjugated backbone.[97] As depicted in Fig. 5a, random terpolymers containing the lowest IID content such as DPP95 (95 mol% DPP and 5 mol% IID) possessed two times higher μ_h^{FET} (5.5×10^{-1} $cm^2 V^{-1} s^{-1}$) value than that of the parent polymer DPP100 (100 mol% DPP and 0 mol% IID) (2.5×10^{-1} $cm^2 V^{-1} s^{-1}$). Under 100% strain, DPP95 also exhibited much higher $\mu_{h\parallel}^{FET}$ (3.5×10^{-2} $cm^2 V^{-1} s^{-1}$) and $\mu_{h\perp}^{FET}$ (5.1×10^{-2} $cm^2 V^{-1} s^{-1}$) values

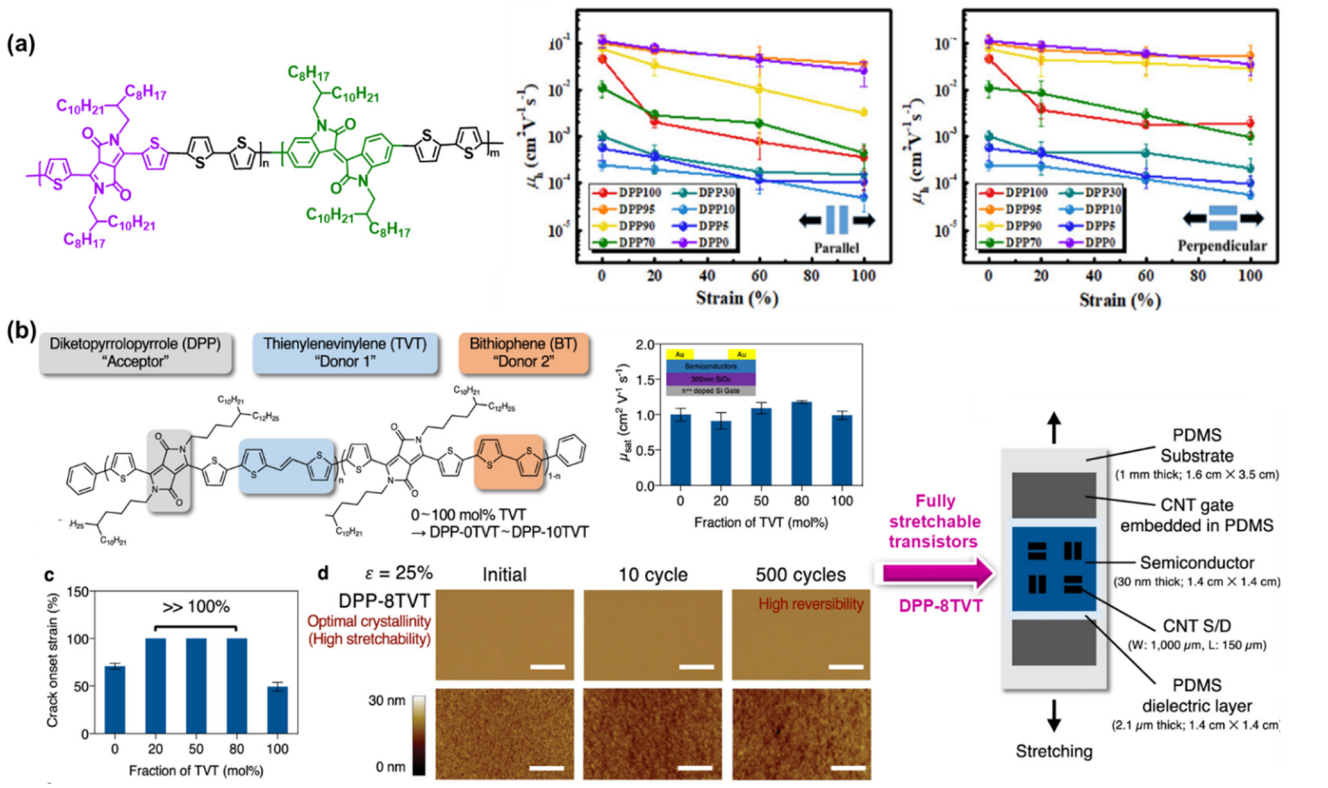

Fig. 5 Intrinsically stretchable semiconducting polymer developed based on the ternary copolymer approach. Chemical structure and mechanical and electrical performances of: (a) random terpolymers based on the diketopyrrolopyrrole-bithiophene (DPP-2T) backbone incorporating different amounts of isoindigo (IID) unit.[97] Copyright: 2020, the American Chemical Society. (b) Advances in DPP-based terpolymer semiconductors with two different fractions of TVT and BT conjugated co-monomers from observing simple semiconductor layers to fully stretchable transistors.[98] Copyright: 2021, Springer Nature.

than the reference parent polymer DPP100 ($\mu_{h\parallel}^{FET}$ = 4 × 10^{-4} cm^2 V^{-1} s^{-1} and $\mu_{h\perp}^{FET}$ = 1.8 × 10^{-4} cm^2 V^{-1} s^{-1}). Another benefit of enriching amorphous features is to provide random terpolymers with a more mobile conformation under mechanical deformation, which preserves effective charge transport pathways under strain. Consequently, DPP95 was shown to yield improved mobility retention at 100% strain, delivering mobility of $>10^{-2}$ cm^2 V^{-1} s^{-1}, which surpasses the performance ($\sim 2 \times 10^{-3}$ cm^2 V^{-1} s^{-1}) of the reference parent DPP100. More encouragingly, the increase in elastic and electrical properties was also obvious as DPP95 showed a much better mechanical performance after 800 stretching-releasing cycles at 60% strain, achieving >20% $\mu_{h\perp}^{FET}$ retention. These results suggest that it is possible to increase the mechanical elasticity of semiconducting polymers for TFT devices without having a deleterious effect on their electronic properties.

Recently, Mun *et al.* proposed a promising strategy for to obtain intrinsically stretchable semiconducting polymers with high mobility and mechanical reversibility against repeated mechanical stress.[98] Specifically, a ternary copolymer composed of the DPP unit as a p-type acceptor, TVT unit as donor 1, and bithiophene (BT) unit as donor 2 was prepared based on various concentrations of two types of constituting co-monomers, which were labelled as DPP-0TVT (0 mol% TVT and 100 mol% of BT) to DPP-10TVT (100 mol% TVT and 0 mol% of BT). As depicted in Fig. 5b, the designed terpolymers with a TVT fraction in the range of 20–80 mol% were found to be stretchable to >100% strain without the formation of cracks. In terms of the mechanical reversibility test, DPP-8TVT remained free from mechanical damage despite 500 continuous cycles of 25% strain, while retaining high charge carrier mobility even after repeated strain. Regardless of the TVT fraction, all the terpolymers showed mobility values of >1 cm^2 V^{-1} s^{-1}, which are comparable to or even greater than that of the regular copolymers with only one type of co-monomer units. As the most prominent sample, the DPP-8TVT film was chosen to fabricate fully stretchable transistor arrays, providing tremendous results such as high robustness and improved fracture resistance, as indicated by the slight degradation in mobility under various mechanical deformations (stretching, twisting, and poking) and a negligible decrease in mobility even after 1000 times deformation under 25% strain, respectively. These satisfactory results enable the design of simple polymers that effectively mitigate the long-standing trade-off between mobility and stretchability. Fascinatingly, this molecular design concept is obviously generalizable, and thus allows the construction of stretchable p-type and n-type terpolymer semiconductors by merely utilizing various combinations of electron donors and acceptors molecules. It was hypothesized that the introduction of two different types of fully conjugated co-monomers causes structural randomness in the backbone, which hinders the formation of larger crystalline domains. Substantially, this controlled ordering at different length scales can improve the fracture resistance upon strain without sacrificing the charge transport.

2.2.4 Symmetric side-chain approach. The early routes for the incorporation of non-conjugated segments in the side chains of polymers focused on the selection of the side chain itself such as the classical alkyl chain size, branch point, and other heterophase segments, which dramatically influence the properties of the resulting modified polymer. The most prominent example of this approach can be observed in the study by Yan *et al.*[101] To enrich more amorphous domains, while maintaining strong aggregation between the polymer chains, which is conducive to promote the stretchability of semiconducting polymers, these authors synthesized modified side-chain polythiophenes with ester-substituted, biaxially conjugated extended semi-2-D side chains of 3-(thiophen-2-yl)-6-(thiophen-3-yl)thieno[3,2-*b*]thiophene-bithiophene (PDCTT2T), and 3-(thiophen-2-yl)-6-(thiophen-3-yl)thieno[3,2-*b*]thiophene-difluorobithiophene (PDCTT2T-F). Benefiting from the synergistic effect of the ester-substituted, biaxially extended conjugation and backbone fluorination, the mobility-stretchability of all four modified polythiophenes improved compared to the prototype RRe P3HT (μ_h^{FET} = 6 × 10^{-7} to 1.4 × 10^{-3} cm^2 V^{-1} s^{-1}).[102] Especially, PDCTT2T-F presented the highest μ_h^{FET} of 0.2 cm^2 V^{-1} s^{-1} due to the fact that the fluorinated backbone exerted higher backbone rigidity than the nonfluorinated backbone, and through coherence with the ester-substituted, biaxially extended side chains, resulted in stronger intramolecular charge transfer. Moreover, as shown in Fig. 6a, PDCTT2T and PDCTT2T-F encouragingly retained decent μ_h^{FET} values, regardless of 800 stretching-releasing cycles at 60% maximum strain, outperforming the reference PDCTT and PDCTT-F without side-chain conjugation, which exhibited a one order decrease in mobility. Wen *et al.* explored the effects of poly(butyl acrylate) (PBA, with various concentrations of 0, 5, 10, 20, and 100 mol%) as the side chain embedded in isoindigo-bithiophene (II2T)-conjugated polymers.[103] The findings for the PII2T-PBA series demonstrate an increase in crack onset strain from 25 to 100%, low elastic modulus from 0.8 to 0.12 GPa, and maintained carrier mobility of 0.06–0.8 cm^2 V^{-1} s^{-1} with an on/off current ratio of over 10^5 depending on the amount of PBA chains, as probed using a top-contact transistor device. Among the mentioned compositions, PII2T-PBA10 was shown to be the most reliable candidate with a stable μ_h^{FET} of 0.08–0.1 cm^2 V^{-1} s^{-1} under 60% strain, which could be maintained during 400 repeated stretching-releasing cycles, as indicated in Fig. 6b. This improved ductility was attributed to the larger free volume of the PBA side chains, which reduced the interchain interactions between the polymer backbones. This finding was consistent with the increase in solubility and decrease in crystallinity observed from the GIXD results.

Alternatively, the hydrogen bonds located in the side chain also played a role in enhancing the mechanical and charge transport performance and facilitating the morphological organization. Ocheje *et al.*[22] incorporated a range of amide compositions (5% to 30%) in DPP-based polymers as a direct approach to promote the intermolecular hydrogen bonding moieties between polymer chains and tune the solid-state morphology (Fig. 6c). Upon the addition of 5 mol% amide side chain, there was an enhancement in the charge mobilities to 2.46 cm^2 V^{-1} s^{-1}, but the further addition of 30 mol% amide gradually decreased the

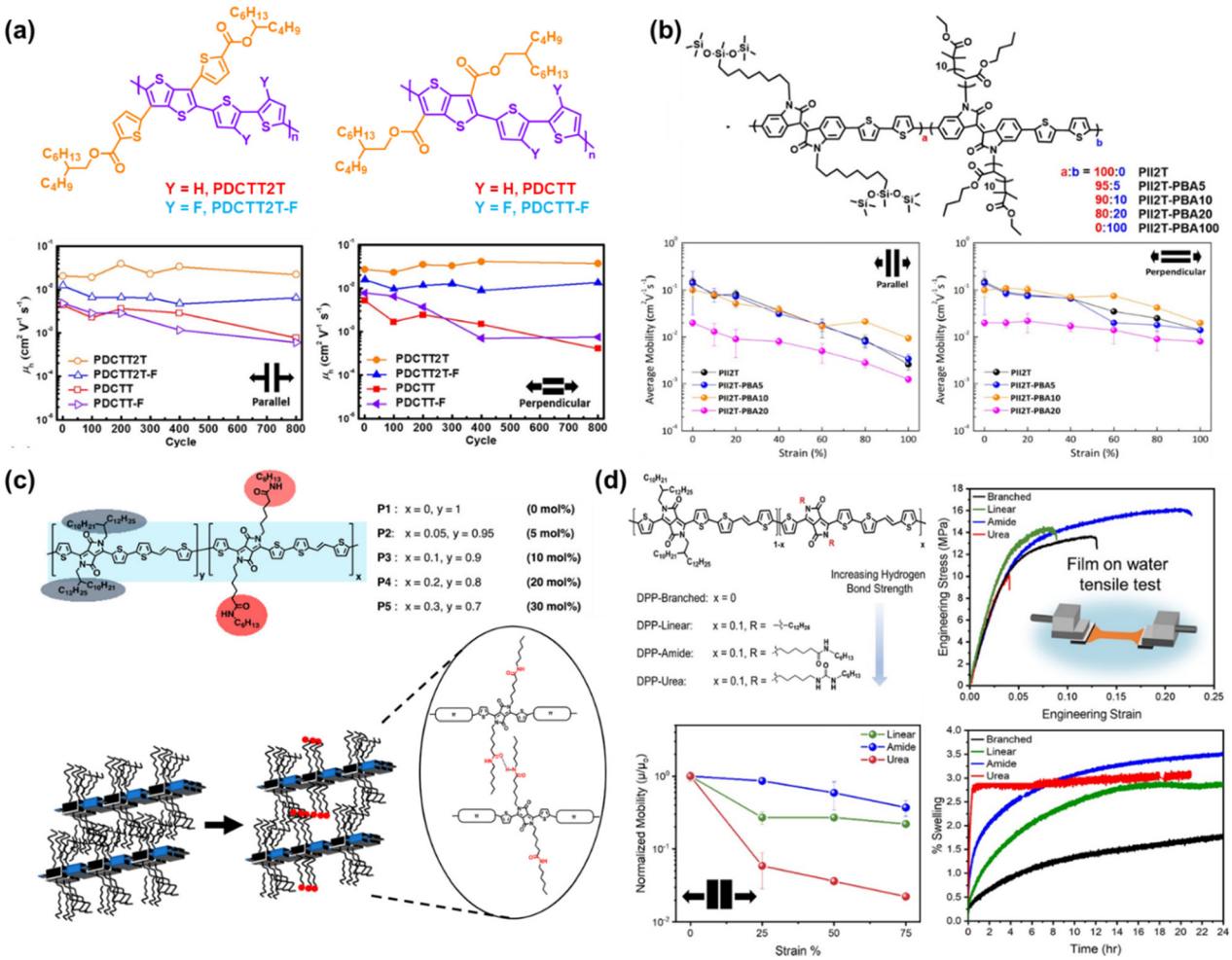

Fig. 6 Side chain engineering based on the grafting approach. (a) Charge mobility-stretchability relationship and chemical structure of PDCTT2T and PDCTT2T-F compared to their non-biaxial counterparts of PDCTT and PDCTT-F, respectively.[101] Copyright: 2021, the American Chemical Society. (b) Influence of the amount of PBA in mol percentage on the PII2T side chain described by charge mobility-stretchability data.[103] Copyright: 2017, the American Chemical Society. (c) Structure of DPP-based conjugated polymers incorporating amide-containing side chains and schematic representation of intermolecular hydrogen bonds formed between adjacent amide-containing side chains.[22] Copyright: 2018, the American Chemical Society.(d) Hydrogen bond strength described in chemical structures of DPP-TVT-based conjugated polymers and its influence on swelling, mechanical, and electrical properties as a function of maximum strain properties.[21] Copyright: 2022, the American Chemical Society.

mobility to 0.59 $cm^2 V^{-1} s^{-1}$. Besides hydrogen bonding, the increase in mobility can be partially influenced by the noncovalent interaction in the conjugated side chain. In comparison, Galuska *et al.*[21] investigated the incorporation of 10% linear alkyl, amide functional, or urea functional side chains in DPP-TVT based statistical copolymers to assess the influence of hydrogen bonding on the mechanical properties of thin films (Fig. 6d). All the polymers demonstrated a similar elastic modulus with the average modulus following the order of DPP-linear > DPP-branched > DPP-urea > DPP-amide. This study showed that the hydrogen bond strength in the side chain is not linearly correlated with ductility, where DPP-urea possessed the highest hydrogen bonding strength but poor ductility due to its crystalline nature in comparison with DPP-amide, which was the best at tolerating deformation due to the disruption in crystalline packing in water. The embrittlement of DPP-urea was further confirmed in the swelling test, where rapid swelling behavior was observed initially but quickly plateaued due to the greater crystallinity. A similar phenomenon was observed in the measurement of the respective charge transport mobility, where the charge transport of DPP-amide decayed by only 14% from 0.199 $cm^2 V^{-1} s^{-1}$ after being strained by 25% in the parallel stretching direction. Considering that the typical maximum strain experienced by human skin is 33%, amide functionalization may be a suitable synthetic strategy to achieve tolerable strain for wearable devices, while maintaining charge transport.

2.2.5 Cross-linking approach. The cross-linking of conjugated polymers has been demonstrated to be an effective strategy to realize the characteristics of elastomers by preventing irrevocable sliding within the polymer chains together with the ability to resist fatigue from multiple stretching. This method can also reduce polymer chain rearrangement and aggregation, thus decreasing the crystallinity. Wang *et al.*

utilized flexible PDMS oligomers for polymer crosslinking to reduce the tensile modulus and improve the fracture strain, and fatigue resistance for a high mobility DPP-based polymer (Fig. 7a).[104] By covalently crosslinking a DPP-based polymer with siloxane oligomers, its elasticity improved, as indicated by the absence of nanocracks after 500 strain-and-release cycles at the maximum strain of 100% and 1000 stretching-releasing cycles with 20% strain. In terms of electrical characteristics, the cross-linked films exhibited an average μ_h^{FET} of 0.66 $cm^2\ V^{-1}\ s^{-1}$ before the strain was applied with an on/off current ratio of above 10^5 and the film could maintain an average $\mu_h^{FET} >$ 0.4 $cm^2\ V^{-1}\ s^{-1}$ after 500 stretching-releasing cycles of 20% strain in the direction perpendicular to the strain direction. However, the average mobility in the direction parallel to the strain was compromised due to the formation of wrinkles. Moreover, the elastic modulus significantly decreased to 0.2 GPa after cross-linking, which contributed to the mechanical toughness of the studied polymers. The studies that also focused on exploiting crosslinking reactions in conjugated polymer networks using crosslinkers with soft and flexible characteristics but not covered in this section can be found in recent reports.[105–108]

The embedding of a cross-linked segment in the side chain conjugated polymer has been demonstrated to be an ideal approach because a high crosslinking density can be easily tuned and disruption of the charge transport is minimized. Thus, the same group investigated the importance of cross-linker crystallinity with respect to morphology, mechanical, and electrical properties of polymers by inserting urethane groups and tertiary carbon atoms into the alkyl backbone of perfluorophenyl azide-based cross-linkers.[109] Similar studies have also been reported.[94,110,111] Here, branched cross-linkers with tertiary carbon are capable of forming an evenly cross-linked network in the polymer blend, stemming from their excellent miscibility, and show a 4-fold increase in fracture strain.[109] Furthermore, a stable μ_h^{FET} of 0.2 $cm^2\ V^{-1}\ s^{-1}$ was achieved under 100% strain, and a stable μ_h^{FET} of 0.1 $cm^2\ V^{-1}\ s^{-1}$ after 2000 stretching-releasing cycles of 25% on fully stretchable organic field-effect transistors. The charge mobility–tensile performance of each specimen in this study is presented in Fig. 7b. Another factor to be considered is the effect of fluorination on the mechanical and electrical properties of conjugated polymers, which was also evaluated by Ocheje *et al.*[112] Their work demonstrated the relationship between a series of fluorination and/or alkylation with benzothiadiazole-based polymer in the solid-state. The crack onset strains of the prepared polymers ranged from as low as 10% for the polymer containing only a fluorinated backbone to as high as 30% elongation for the polymer containing an alkoxy-appended backbone. Ultimately, fluorination embrittled the conjugated polymer thin films, whereas alkylation softened them.

2.2.6 Y-Shaped side-chain approach. The Y-shaped approach focuses on the modification of linear carbon chains after a bifurcate is formed. A systematic study on IID-based polymers containing branched side chains with an adjustable linear carbon spacer unit branching from a carbosilane group was conducted by Wu *et al.*[113] In detail, PII2TC6 and PII2TC8 consisting of an isoindigo-bithiophene main chain and carbosilane side chain with a six or eight linear spacer plus two hexyl or octyl chains, respectively, were synthesized and assessed. The ductility

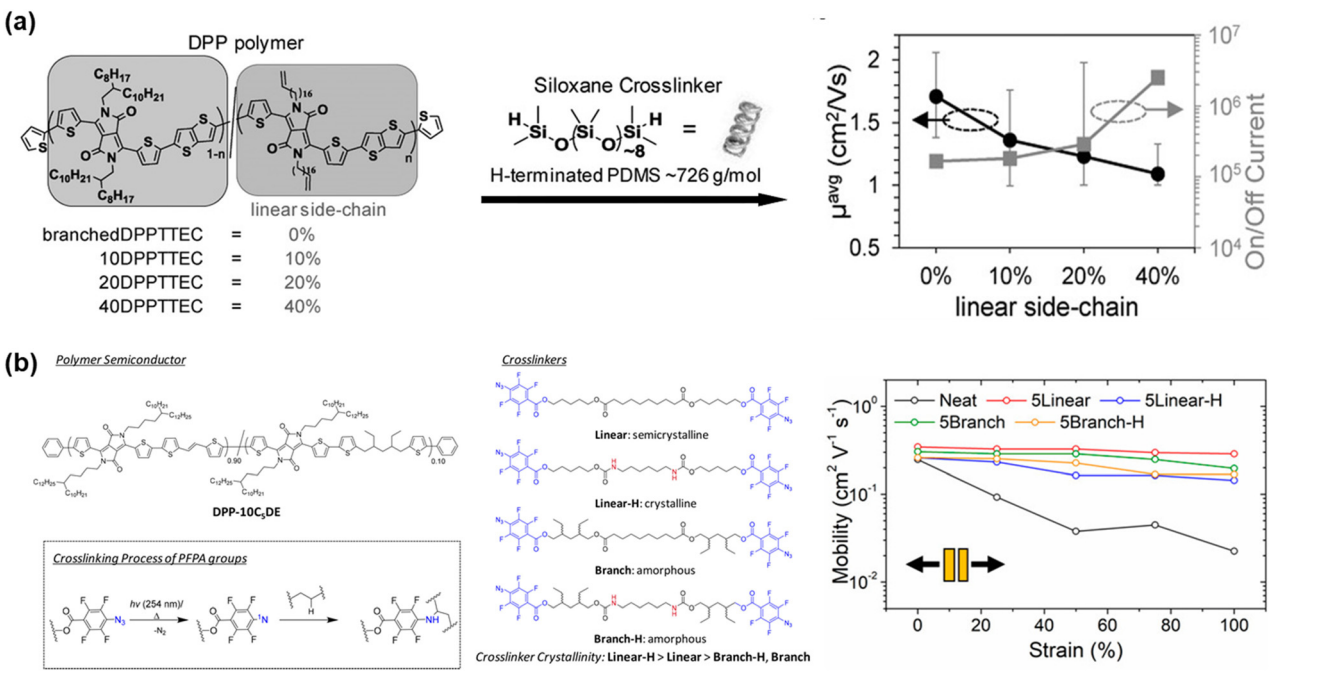

Fig. 7 Side chain engineering based on crosslinking approach. Chemical structure and the retention of mobility properties of the polymers in the stretched state. (a) DPP-based random co-polymer containing cross-linkable linear side-chains and linear H-terminated PDMS crosslinker.[104] Copyright 2016, Wiley-VCH. (b) Introduction four types of cross-linkers in DPP-based polymer.[109] Copyright: 2019, the American Chemical Society.

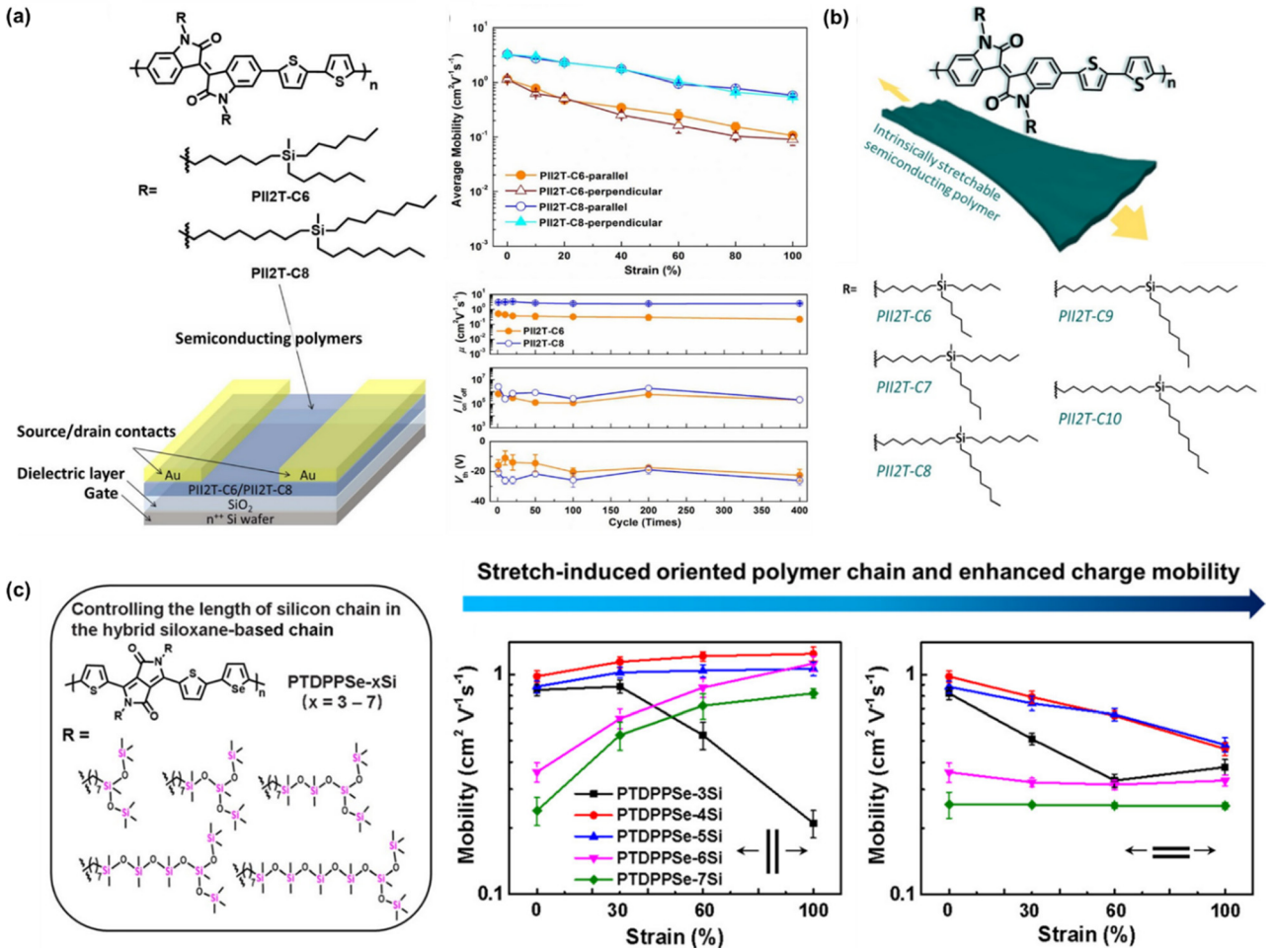

Fig. 8 Modulating the mechanical-electrical properties of conjugated polymers *via* side chain engineering based on y-shaped approach. (a) Average field-effect mobility stretched in the parallel and perpendicular directions and the mechanical-mobility resistance of the of the PII2T-C6 and PII2T-C8 thin films under repeated 400 stretching/releasing cycles with a maximum strain of 60% controlled parallel to the strain direction.[113] Copyright: 2016, the American Chemical Society. (b) Chemical structures of PII2T-based polymers with manipulated length of carbosilane side chains, charge mobility distribution in both parallel and perpendicular directions of PII2T with carbon position ranging from C6 to C10 and normalized mobility in the parallel direction of the studied polymer thin films under strain.[114] Copyright: 2019, the American Chemical Society. (c) PTDPPSe-based conjugated polymer bearing different lengths of silicon chain.[119] Copyright: 2022, the American Chemical Society.

measurement of PII2TC6 and PII2TC8 exhibited an impeccable mechanical performance with significant reduction in the tensile modulus at 0.43 and 0.27 GPa, respectively. The average charge carrier mobility upon annealing obtained from both specimens was 2.48 and 5.56 $cm^2\ V^{-1}\ s^{-1}$, respectively, with the maximum value of 8.06 $cm^2\ V^{-1}\ s^{-1}$ achieved by PII2TC8. A similar rate of charge transport characteristics was observed under a single stretching in the parallel and perpendicular directions (Fig. 8a). The charge mobility of the PII2TC6 thin film decreased from 1.14 to 0.11 $cm^2\ V^{-1}\ s^{-1}$ as the strain level increased to 100%, while the PII2T-C8 thin film exhibited a higher initial charge mobility of 3.24 $cm^2\ V^{-1}\ s^{-1}$ with a sustained value above 1 $cm^2\ V^{-1}\ s^{-1}$ at 60% strain due to its better thin film ductility and denser molecular packing structure (*i.e.*, shorter π–π stacking distance). Furthermore, the PII2T-C6 and PII2T-C8 thin films showed stable performances without significant changes in their mobility, on/off ratio, and threshold voltage during 400 stretch-and-release cycles of 100% strain. This achievement demonstrated that the newly designed IID-based polymer thin film with excellent ability to maintain stability and reproducibility under 60% tensile strain exhibits high potential to be integrated in future skin-inspired wearable electronics.

The effects of the carbon spacer present in the branch was investigated further by Chiang *et al.* (Fig. 8b).[114] This group managed to improve the findings based on the work by Wu *et al.* by further repositioning the carbona of the side chain from 6 (PII2T-C6) to 10 carbons (PII2T-C10) to optimize the charge-transport behavior and the mechanical properties of semiconducting polymer thin films. By increasing the side chain length, the thin film modulus could be further reduced to 250 MPa with an almost unchanged μ_h^{FET} upon stretching of 1 $cm^2\ V^{-1}\ s^{-1}$ at 100% strain in both the parallel and perpendicular directions. In contrast, PII2T-C8 showed a higher initial mobility but it notably decreased upon stretching (0.7 $cm^2\ V^{-1}\ s^{-1}$ at 100%). The initial mobility of PII2T-C10 was not as high as that

of PII2T-C8 due to the disturbance of its backbone organization. Additionally, the length of the carbon side chain and the odd-even effect of the carbon position becomes a factor. Cracks could be seen in the PII2T-C6 and PII2T-C7 thin films under 100% strain but were significantly less in PII2T-C10. Polymers with even-numbered carbosilane side chains (C6, C8, and C10) possess smaller π–π stacking than the side chains with an odd carbon number (C7 and C9), and thus a higher mechanical and electrical performance can be achieved in even-numbered side chains.

Departing from the commonly used Y-shaped alkyl side chains, hybrid siloxane-based side chains are more easily deformed owing to their long bond lengths and large bond angles, together with low internal torsional potential barriers.[115–117] Mei *et al.* demonstrated the effectiveness of novel siloxane-terminated solubilizing groups as a side chain in an isoindigo-based conjugated polymer (PII2T-Si) for promoting the field-effect mobility by inducing a denser π–π spacing and a larger crystalline coherence length.[28] The hole mobility of PII2T-Si was 2.48 $cm^2 V^{-1} s^{-1}$, which is 4 times greater than that of the reference polymer with a branched alkyl side chain (PII2T-Ref). This was explained by the polymer packing, where the new polymer exhibited a π–π stacking distance of 3.58 Å, while PII2T-Ref showed a distance of 3.76 Å. Starting from this discovery, other researchers tried to modify the conjugated polymer Y-shaped side chain by incorporating hybrid siloxane-based side chains.[87,118] In the latest study by Ding *et al.*, they introduced a novel side chain engineering strategy to realize stretch-induced enhancement of the molecular orientation and charge transport in donor–acceptor conjugated polymers.[119] Specifically, five conjugated polymers with a controlled hybrid siloxane-based side chain length were grafted on the backbone of poly-diketo-pyrrolopyrrole-selenophene: PTDPPSe-*x*Si (x = 3–7). Considering the superior flexibility of silicon chains compared carbon chains, a series of polymers showed a progressively lower elastic modulus and increased fracture strain by increasing the silicon chain length, whereas the charge mobility could be enhanced with an appropriate increase in the silicon chain length (Fig. 8c). Interestingly, the charge mobilities parallel to the stretching direction for PTDPPSe-4Si, PTDPPSe-5Si, and PTDPPSe-6Si were all above 1 $cm^2 V^{-1} s^{-1}$ at 100% strain, which were higher than that in their unstretched states. This enhancement in charge mobility is attributed to the excellent ductility and high strain-induced alignment of the polymer chains. Different from most other studies on controlling the carbon chain length in hybrid siloxane-based chains, this technique provides an alternative for manipulating the silicon chain length in hybrid siloxane-based chains.

2.2.7 Asymmetric side-chain approach. Asymmetric side-chain engineering in isoindigo-bithiophene based conjugated polymers has been reported to modulate the three-dimensional charge-transport pathways to enhance the charge mobility.[120,121] By the simultaneous incorporation of linear and branched side chains, interchain stacking can be suppressed as a result of the increased side-chain packing. This result will be very beneficial in yielding a polymer film with high ductility. Lin *et al.* developed a series of PII2T (P1–P3) and PII2TF (P4–P6) as polymer backbones with asymmetric side chains, consisting of carbosilane side chains (Si-C8), siloxane-terminated side chains (SiO-C8), and decyltetradecane side chains (DT), as shown in Fig. 9a.[122] Owing to the geometric dissimilarity between the side chains, in which both SiO-C8 and Si-C8 have the same eight-carbon spacer before the branching point but with distinct branched chains after the branching point, the DT possessed a shorter spacer before the branching point, which impacts the apparent asymmetric side-chain differences in the molecular stacking and orientation of the derived polymers. Thus, it will greatly affect the resultant mobility and stretchability. The asymmetric SiO-C8/Si-C8 side chains enabled the derived polymers to possess the most balanced bimodal orientation, providing the greatest μ_h^{FET} values of 3.49 $cm^2 V^{-1} s^{-1}$ (P1) and 1.39 $cm^2 V^{-1} s^{-1}$ (P4) in their respective series. Through the Derjaguin–Muller–Toporov (DMT) model for AFM topography, the elastic modulus of PII2T was confirmed to be (0.55, 0.55, and 0.51 GPa) lower than that of the fluorinated P4–P6 (0.56, 0.67, and 0.71 GPa), respectively. The higher elastic modulus in P4–P6 is due to the higher backbone rigidity in the fluorination-based polymer. Benefitting from the advantages of twisted packing induced by the fluorinated backbone, the degree of crystallinity was reduced, indicating a favorable enhancement in stretchability and mechanical durability. Consequently, the modification of the asymmetric Si-C8/DT side chains and PII2T with a fluorinated backbone (P6) resulted in the best mobility preservation of 81% at 100% strain with the stretching force

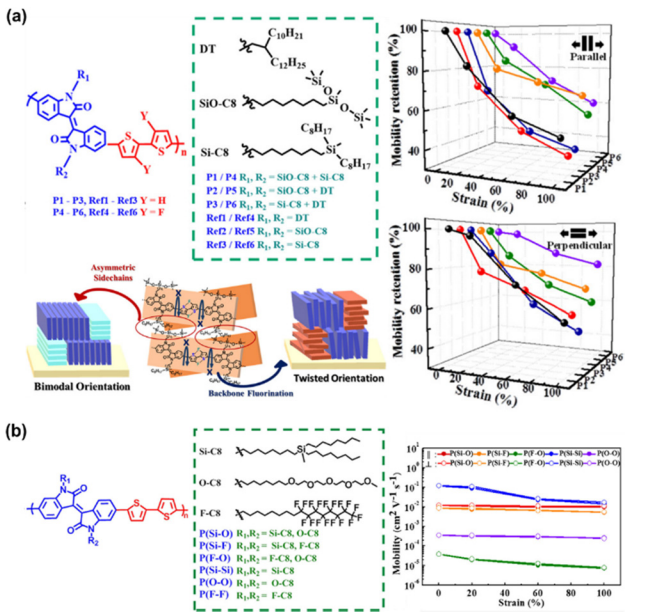

Fig. 9 Tuning the electrical-mechanical properties of conjugated polymers *via* asymmetric side-chain engineering. (a) Asymmetrical side-chain engineering of IID-based polymers structure; illustration of the effects of the asymmetric side-chain design and backbone fluorination on chain packing; and the mobility retention of these polymers with different strains and with the stretching force parallel and perpendicular to the charge-transporting direction.[122] Copyright: 2019, the American Chemical Society. (b) Structure of isoindigo-bithiophene (II2T)-based conjugated polymers with three types of side chains and the orthogonal hole mobilities values of the stretched polymer films with strain ranging from 0 to 100%.[123] Copyright: 2021, the American Chemical Society.

perpendicular to the charge-transport direction. Moreover, it presented 90% mobility retention after 400 stretching-releasing cycles with 60% strain, greatly exceeding that (36%) of its non-fluorinated counterpart (P3). Aiming to expand the combinations with other side-chain segments to control the carrier mobility-stretchability properties, Yen *et al.* formulated a series of asymmetric side chains in PII2T-based conjugated polymers: carbosilane side-chain, semi-fluorinated side-chain, and oligoether side-chain (Fig. 9b).[123] Among the specimens, the carbosilane side-chain exhibited the lowest modulus value of 0.45 GPa and the most formidable μ_h^{FET} of 0.56 $cm^2\ V^{-1}\ s^{-1}$ together with retained charge mobility after 1000 stretching-releasing cycles of 60% strain.

With the exception of the block copolymer approach, seven approaches for manipulating semiconducting polymer structures have been successful in providing satisfactory load mobility ($\mu_h^{FET} > 1\ cm^2\ V^{-1}\ s^{-1}$) even under 100% mechanical stretching. However, the modified semiconducting materials still have a high elastic modulus (>0.1 GPa), indicating the inadequate deformability and ductility of thin films. Based on the range of limitations of this review, the block copolymer, CBS, and symmetric side-chain approaches can achieve an elastic modulus close to or lower than 0.1 GPa. To make the comparison much more convenient, in Table 1, we also compare the performances of intrinsically stretchable semiconducting polymers.

2.3 Stretchable semiconducting polymer blends

Compared with the elegantly structured semiconductor polymers modified through complicated synthetic procedures, blending semiconducting polymers with other conjugated polymers, small molecules, or soft-building block polymers is presented as the most favorable method because sometimes it offers an economic, simpler, or better alternative. Introducing an appropriate secondary component *via* physical blending leads to polymer dilution, which changes the morphology, cohesion and viscosity, among other physical characteristics, ultimately impacting the electromechanical properties of thin film polymers. However, a dilemma in this method in achieving deformability, typically resulting in a deterioration in the charge transport, and *vice versa*.[124] This is because if only the simple blending method is employed without promoting any suitable morphology, there may be a significant reduction in charge carrier mobility due to the charge transport impediment between the semiconducting domains by the insulating component. Thus, to solve this issue, researchers considered the influence of the processing approach,[73,125–128] thickness,[129] and nanoconfinement[32,130,131] on improving the stretchability of high-mobility polymer blends. As expected, these considerations led to the successful production of blended semiconducting polymers, which can actually effortlessly alter and even optimize the mechanical ductility, mobility/molecular ordering, and stability of conjugated polymer-FETs substantially, together with newly emerging polymer blend characteristics.

In the simplest case, the widely studied semiconducting blend composed of 0.75 wt% P3HT:poly(dimethylsiloxane) (PDMS), where P3HT is prepared *via* ''pre-deposition processing'' became more resistance to external strain and exhibited an improved electrical performance up to 2 times that of the non-PDMS-containing sample and 44 times greater than that of the untreated P3HT (Fig. 10a).[73] Meanwhile, no charge transport behavior was observed for pristine P3HT:PDMS blends. The use of the ''pre-deposition processing'' technique is known to facilitate enhanced P3HT alignment/ordering/crystallinity with a concomitant improvement in charge carrier mobility.[132,133] As analyzed by UV-vis absorption, the samples were red-shifted following the sequence of pristine P3HT, ultrasonicated P3HT/PDMS, and poor solvent/ultrasonicated P3HT/PDMS, implying that agglomeration was induced by the stronger molecular interaction between the two blend components as a result of their improved crystallinity. This result was further supported by the narrower full width at half-maximum (FWHM) of the XRD peaks. The poor miscibility between PDMS and P3HT was also observed *via* Hansen solubility parameter analysis, leading to the formation of dendritic aggregates by P3HT. However, this research is still in its infancy given that the performance of thin-film transistors upon stretching has not been evaluated to date.

Given that this versatile approach has no limitations on the material chosen, Zhang *et al.* proposed the fabrication of transparent and elastic semiconductor films by blending only a small amount (less than 1 wt%) of either p-type or n-type commercial semiconductors in PDMS as the transparent stretchable insulating component.[134] P3HT and poly[2,5-(2-octyldodecyl)-3,6-diketopyrrolopyrrole-*alt*-5,5-(2,5di(thien-2-yl)-thieno [3,2-*b*]thiophene)] (DPP-DTT) were used as p-type semiconducting polymers, whereas poly(2,5-bis(2-octyldodecyl)-3,6-di(pyridin-2-yl)-pyrrolo[3,4-*c*]pyrrole-1,4(2*H*,5*H*)-dione-*alt*-2,2′-bithiophene) (DPPDPyBT) was used as an electron transport (n-channel) semiconducting polymer. With appropriate semiconductor weight fractions, it was observed that the mobility of 0.49 wt% P3HT/PDMS, 0.83 wt% DPP-DTT/PDMS, and 0.62 wt% DPPDPyBT/PDMS was 0.23, 1.75, and 1.34 $cm^2\ V^{-1}\ s^{-1}$, respectively. All of them exhibited an enhancement by ~10-fold, 2-fold, and 3-fold in mobility compared to the control samples (100 wt%) of P3HT, DPP-DTT, and DPPDPyBT, respectively. The electrical-mechanical performance of semiconductor/insulating polymer blend films under 100% strain parallel to the charge transport direction was evaluated *via* the delamination–stretching–relamination process,[33,135] resulting in a slight decrease in charge carrier mobility, while the transfer curve was unaffected. Owing to its good transparency, biocompatible, low cost, and ease of fabrication, commercial PDMS is often selected by researchers as an insulating polymer in these types of binary blend systems. The detailed mechanical and electrical behavior of semiconducting polymer-*blended*-PDMS films are further summarized in Table 2.

Liu *et al.* investigated the influence of molecular aggregation on the film morphology of conjugated polymer poly(indacenodithiophene-*co*-benzothiadiazole) (IDTBT)-blended-elastomer polystyrene-*block*-poly(ethylene-ran-butylene)-*block*-polystyrene (SEBS) at much broader parameter choices, including two types of high-boiling-point (bp) solvents such as toluene (Tol) and chlorobenzene (CB) and fast solvent evaporation from low-bp chloroform (CF) (Fig. 10b).[136] When a solvent with high-bp was utilized as the processing solvent (Tol and CB), phase

Table 1 Summary of the performance of intrinsically stretchable semiconducting polymers reported in the literature

Design Method	Materials	Engineering details	Average mobility ($cm^2 V^{-1} s^{-1}$)			Mechanical properties			Ref.
			Before	After		Stretchability (% strain)	Elastic modulus (GPa)	Durability	
				Parallel	Perpendicular				
Block copolymer approach	P3HT	Diblock copolymers	1×10^{-2}	—	—	13	0.028	—	77
	$P3HT_{35}$-PE_{65}		5×10^{-2}	—	—	660	0.24	—	
	P3HT	Diblock copolymers	0.079	2.2×10^{-4} at 100% strain	1.1×10^{-4} at 100% strain	—	0.93[d]	—	79
	P3HT-*b*-PBA_{3k}[a]		0.073	7.9×10^{-4} at 100% strain	6.9×10^{-4} at 100% strain	—	0.63[d]	—	
	P3HT-*b*-PBA_{6k}[a]		0.061	0.025 at 100% strain	0.025 at 100% strain	—	~0.35[d]	$\mu_{h\parallel}^{FET}$ and $\mu_{h\perp}^{FET}$ ≥ 0.01 $cm^2 V^{-1} s^{-1}$ under 100% strain for 1000 cycles	
	P3HT-*b*-PBA_{12k}[a]		0.014	2.1×10^{-3} at 100% strain	1.9×10^{-3} at 100% strain	—	0.19[d]	—	
	P3HT-*b*-PMA-*b*-P3HT	ABA triblock copolymer	1.7×10^{-4}	—	—	140[d]	0.006[d]	—	81
	P3HT-*b*-P3SiHT[a]	Diblock copolymer	5.61×10^{-3}	—	—	25.6	0.056[b]	—	83
	P3HT-*b*-P3SiHT-*b*-P3HT	ABA triblock copolymer	5.14×10^{-3}	—	—	118	0.003	—	
Molecular spacer approach	P3HTT-DPP-10[a]	Fully conjugated semi-random	9.29×10^{-4}	—	—	COS[a]: 10	0.32[c]	—	92
	10% T-10-T[a]	Semi-random polymers with CBS	2.53×10^{-4}	—	—	COS: >80	0.13[b] 0.15[c]	—	
	20% T-10-T		1.06×10^{-4}	—	—	COS: >80	0.32[b] 0.52[c]	—	
	30% T-10-T		3.55×10^{-4}	—	—	COS: >80	0.33[b] 0.60[c]	—	
	Ref-polymer[a]	Modified chain length and rigidity of CBS	2.1	0.9 at 100% strain	0.7 at 100% strain	COS: 25[c]	1.1[c]	$\mu_{h\parallel}^{FET}$ = ~0.6 and $\mu_{h\perp}^{FET}$ = ~0.08 $cm^2 V^{-1} s^{-1}$ under 50% strain for 100 cycles	93
	C12-DPP/TVT		1.3	1.0 at 100% strain	0.6 at 100% strain	COS: 100[c]	0.13[c]	$\mu_{h\parallel}^{FET}$ = ~0.36 and $\mu_{h\perp}^{FET}$ = ~0.8 $cm^2 V^{-1} s^{-1}$ under 50% strain for 100 cycles	
	PDPPTT	Introducing conjugated rigid fused-rings with optimized bulky side groups	0.76	0.07 at 75% strain	0.11 at 75% strain	COS: 20[c]	—	$\mu_{h\parallel}^{FET}$ = 0.06 and $\mu_{h\perp}^{FET}$ = ~0.4 $cm^2 V^{-1} s^{-1}$ under 25% strain for 500 cycles	95
	PDBTTT-10%		0.7	0.03 at 75% strain	0.06 at 75% strain	COS: 40[c]	—	$\mu_{h\parallel}^{FET}$ = 0.3 and $\mu_{h\perp}^{FET}$ = ~0.5 $cm^2 V^{-1} s^{-1}$ under 25% strain for 500 cycles	
	PID-3T-OC12-10%[a]		0.9	0.27 at 75% strain	0.2 at 75% strain	COS: 60[c]	—	$\mu_{h\parallel}^{FET}$ = 0.22 and $\mu_{h\perp}^{FET}$ = ~0.38 $cm^2 V^{-1} s^{-1}$ under 25% strain for 500 cycles	

Table 1 (*continued*)

Design Method	Materials	Engineering details	Average mobility ($cm^2\ V^{-1}\ s^{-1}$) Before	After Parallel	After Perpendicular	Mechanical properties: Stretchability (% strain)	Elastic modulus (GPa)	Durability	Ref.
Terpolymerization approach	G1[a]	Introducing PAM-coupled alkyl side chains into the polymer backbone	0.52	0.030 at 100% strain	0.048 at 100% strain		0.85	—	97
	G2[a]		0.26	0.038 at 100% strain	0.052 at 100% strain		0.80	$\mu_{h\parallel}^{FET} = 3 \times 10^{-3}$ and $\mu_{h\perp}^{FET} = 2 \times 10^{-4}$ $cm^2\ V^{-1}\ s^{-1}$ under 60% strain for 400 cycles	
	G3[a]		0.38	0.10 at 100% strain	0.12 at 100% strain		0.76	$\mu_{h\parallel}^{FET} = 9 \times 10^{-3}$ and $\mu_{h\perp}^{FET} = 4 \times 10^{-3}$ $cm^2\ V^{-1}\ s^{-1}$ under 60% strain for 400 cycles	
	G4[a]		0.15	0.011 at 100% strain	0.031 at 100% strain		0.71	—	
	G5[a]		0.21	0.021 at 100% strain	0.043 at 100% strain		0.36	$\mu_{h\parallel}^{FET} = 0.02$ and $\mu_{h\perp}^{FET} = 3 \times 10^{-3}$ $cm^2\ V^{-1}\ s^{-1}$ under 60% strain for 400 cycles	
	DPP-8TVT	A–D–A–D′ type	>1	>1 at 100% strain	>1 at 100% strain	COS: ≫ 100	0.65	500 stretching/releasing cycles at 25% strain	98
Symmetric side-chain approach	PDCTT2T	Biaxially extended conjugated side chain	0.06	2×10^{-3} at 100% strain	4×10^{-3} at 100% strain	—	—	$\mu_{h\parallel}^{FET} = 0.02$ and $\mu_{h\perp}^{FET} = 0.03$ $cm^2\ V^{-1}\ s^{-1}$ under 60% strain for 800 cycles	101
	PDCTT2T-F		0.02	2.5×10^{-4} at 100% strain	2.5×10^{-3} at 100% strain	—	—	$\mu_{h\parallel}^{FET} = 6 \times 10^{-3}$ and $\mu_{h\perp}^{FET} = 1.5 \times 10^{-3}$ $cm^2\ V^{-1}\ s^{-1}$ under 60% strain for 800 cycles	
	PII2T	Introducing soft side chain	0.15	1.4×10^{-3} at 100% strain	2.6×10^{-4} at 100% strain	COS: <10[d]	0.80[d]	—	103
	PII2T-PBA5		0.14	1.4×10^{-3} at 100% strain	3.4×10^{-4} at 100% strain	COS: ∼20[d]	0.63[d]	—	
	PII2T-PBA10		0.10	0.02 at 100% strain	9.4×10^{-4} at 100% strain	COS: ∼40[d]	0.57[d]	$\mu_{h\parallel}^{FET} = 8 \times 10^{-3}$ and $\mu_{h\perp}^{FET} = 0.01$ $cm^2\ V^{-1}\ s^{-1}$ under 60% strain for 400 cycles	
	PII2T-PBA20		0.021	8.1×10^{-3} at 100% strain	1.2×10^{-4} at 100% strain	COS: 60[d]	0.12[d]	—	
	20DPPTTEC	Crosslinked with PDMS oligomer	1.37	—	—	COS: >150	0.28[d]	Stable $\mu_{h\perp}^{FET} \approx 0.4$ $cm^2\ V^{-1}\ s^{-1}$ under 20% strain for 500 cycles	104
	DPP-10C_5DE	Tuning of the cross-linker's crystallinity	0.25	0.02 at 100% strain	0.02 at 100% strain	Pristine COS: 25[b] Annealed[e] COS: 25[b]	Pristine: 0.225[b] Annealed[e]: 0.225[b]	$\mu_{h\parallel}^{FET} = 0.01$ and $\mu_{h\perp}^{FET} = 0.03$ $cm^2\ V^{-1}\ s^{-1}$ under 25% strain for 2000 cycles	109
	5Linear[a]		0.34	0.29 at 100% strain	0.02 at 100% strain	Pristine COS[a]: 50[b] Annealed[e] COS[a]: 100[b]	Pristine: 0.205[b] Annealed[e]: 0.234[b]	$\mu_{h\parallel}^{FET} = 0.01$ and $\mu_{h\perp}^{FET} = 0.06$ $cm^2\ V^{-1}\ s^{-1}$ under 25% strain for 2000 cycles	
	5Linear-H[a]		0.26	0.14 at 100% strain	0.05 at 100% strain	Pristine COS[a]: 50[b]	Pristine: 0.234[b]	$\mu_{h\parallel}^{FET} = 0.05$ and $\mu_{h\perp}^{FET} = 0.03$ $cm^2\ V^{-1}\ s^{-1}$ under 25% strain for 2000 cycles	

Table 1 (*continued*)

Design Method	Materials	Engineering details	Average mobility ($cm^2\ V^{-1}\ s^{-1}$) Before	After Parallel	After Perpendicular	Mechanical properties: Stretchability (% strain)	Elastic modulus (GPa)	Durability	Ref.
	5Branch[a]		0.30	0.20 at 100% strain	0.03 at 100% strain	Annealed[e] COS[a]: 75[b] Pristine COS[a]: 75[b]	Annealed[e]: 0.230[b] Pristine: 0.236[b]	$\mu_{h\parallel}^{FET}$ = 0.03 and $\mu_{h\perp}^{FET}$ = 0.12 $cm^2\ V^{-1}\ s^{-1}$ under 25% strain for 2000 cycles	
	5Branch-H[a]		0.26	0.17 at 100% strain	0.04 at 100% strain	Annealed[e] COS[a]: 100[b] Pristine COS[a]: 75[b]	Annealed[e]: 0.204[b] Pristine: 0.2[b]	$\mu_{h\parallel}^{FET}$ = 0.03 and $\mu_{h\perp}^{FET}$ = 0.11 $cm^2\ V^{-1}\ s^{-1}$ under 25% strain for 2000 cycles	
						Annealed[e] COS[a]: >100[b]	Annealed[e]: 0.215[b]		
Y-Shape approach	PII2T-C6	Incorporation of branched alkyl side chain	1.14	0.11 at 100% strain	0.09 at 100% strain	>100	0.430[c]	$\mu_{h\parallel}^{FET}$ = 0.2 $cm^2\ V^{-1}\ s^{-1}$ under 60% strain for 400 cycles	113
	PII2T-C8		3.24	0.58 at 100% strain	0.54 at 100% strain	>100	0.270[c]	$\mu_{h\parallel}^{FET} \geq 1 cm^2\ V^{-1}\ s^{-1}$ under 60% strain for 400 cycles	
	PII2T-C6	Incorporation of branched alkyl side chain	2.48	0.2 at 100% strain	0.09 at 100% strain	—	0.565[d]	—	114
	PII2T-C7		2.06	0.1 at 100% strain	0.09 at 100% strain	—	0.465[d]	—	
	PII2T-C8		4.67	0.7 at 100% strain	0.7 at 100% strain	—	0.375[d]	—	
	PII2T-C9		0.92	0.15 at 100% strain	0.09at 100% strain	—	0.280[d]	—	
	PII2T-C10		2.23	2.0 at 100% strain	2.2 at 100% strain	—	0.250[d]	$\mu_{h\parallel}^{FET}$ and $\mu_{h\perp}^{FET}$ = ~1 $cm^2\ V^{-1}\ s^{-1}$ under 60% strain for 500 cycles	
	PTDPPSe-3Si	Grafting hybrid siloxane-based side chains	0.85	0.21 at 100% strain	0.38 at 100% strain	—	0.378[b]	—	119
	PTDPPSe-4Si		0.98	1.24 at 100% strain	0.46 at 100% strain	—	0.264[b]	—	
	PTDPPSe-5Si		0.88	1.08 at 100% strain	0.48 at 100% strain	—	0.186[b]	—	
	PTDPPSe-6Si		0.36	1.12 at 100% strain	0.33 at 100% strain	—	0.129[b]	—	
	PTDPPSe-7Si		0.24	0.82 at 100% strain	0.25 at 100% strain	—	0.087[b]	—	
Asymmetric side-chain approach	P1[a]	Inserting asymmetric side chains	0.33	0.16 at 100% strain	0.18 at 100% strain	—	0.55	—	122
	P2[a]		0.54	0.21 at 100% strain	0.32 at 100% strain	—	0.55	—	
	P3[a]		0.60	0.24 at 100% strain	0.29 at 100% strain	—	0.51	$\mu_{h\parallel}^{FET}$ = 0.15 and $\mu_{h\perp}^{FET}$ = 0.2 $cm^2\ V^{-1}\ s^{-1}$ under 60% strain for 400 cycles	
	P4[a]		0.21	0.14 at 100% strain	0.12 at 100% strain	—	0.56	—	
	P5[a]		0.22	0.12 at 100% strain	0.14 at 100% strain	—	0.67	—	
	P6[a]		0.26	0.16 at 100% strain	0.21 at 100% strain	—	0.71	$\mu_{h\parallel}^{FET}$ = 0.18 and $\mu_{h\perp}^{FET}$ = 0.2 $cm^2\ V^{-1}\ s^{-1}$ under 60% strain for 400 cycles	
	P(Si–O)[a]	Inserting asymmetric side chains	0.012	9.8×10^{-3} at 100% strain	0.011 at 100% strain	>80	0.45	Almost unchanged μ_h^{FET} under 60% strain for 1000 cycles	123
	P(Si–F)[a]		8.7×10^{-3}	5.3×10^{-3} at 100% strain	5.3×10^{-3} at 100% strain	~60	2.09	—	

Table 1 (*continued*)

Design Method	Materials	Engineering details	Average mobility ($cm^2 V^{-1} s^{-1}$)			Mechanical properties		Durability	Ref.
			Before	After		Stretchability (% strain)	Elastic modulus (GPa)		
				Parallel	Perpendicular				
	P(F–O)[a]		3.8×10^{-5}	7.6×10^{-6} at 100% strain	8.0×10^{-6} at 100% strain	~20	2.79	—	

[a] Abbreviations: COS = crack onset strain; ref-polymer = DPP-based random copolymers incorporated with 10 mol% ethylene as the conjugation breaker; G1 = polymer with DPP-thiophenevinylenethiophene (PDPPTVT) backbone with side chains consisting of methyl(8-bromooctyl)dioctylsilane (SiC8); G2 = PDPPTVT-SiC8-5% of poly(acryl amide) (PAM); G3 = PDPPTVT-SiC8-9% PAM; G4 = PDPPTVT-SiC8-16% PAM; G5 = polymer with DPP-selenophene (PDPPSe) backbone with side chains consisting of methyl(8-bromooctyl)dioctylsilane (SiC8) and 5% of poly(acryl amide) (PAM); 5Linear = neat with 5 wt% semi-crystalline perfluorophenyl azide-based cross-linker blend; 5LinearH = neat with 5 wt% highly crystalline perfluorophenyl azide-based cross-linker blend; 5Branch = neat with 5 wt% amorphous perfluorophenyl azide-based cross-linker blend ($T_g = -21.9$ °C); P1 = SiOC8 and Si-C8 side chain engineered in isoindigo-bithiophene (PII2T) backbone; P2 = DT/SiO-C8 side chain engineered in isoindigo-bithiophene (PII2T) backbone; P3 = DT/Si-C8 side chain engineered in isoindigo-bithiophene (PII2T) backbone; P4 = SiOC8 and Si-C8 side chain engineered in isoindigo-difluorobithiophene (PII2TF) backbone; P5 = DT/SiO-C8 side chain engineered in isoindigo-difluorobithiophene (PII2TF) backbone; P6 = DT/Si-C8 side chain engineered in isoindigo-difluorobithiophene (PII2TF) backbone; P(Si–O) = carbosilane/oligoether side chains engineered in isoindigo-bithiophene (II2T)-based polymer; P(Si–F) = carbosilane/semi-fluorinated side chains engineered in isoindigo-bithiophene (II2T)-based polymer; and P(F–O) = semi-fluorinated/oligoether side chains engineered in isoindigo-bithiophene (II2T)-based polymer. [b] Measured by film-on-water tensile test. [c] Measured by film-on-elastomer tensile test. [d] Measured by buckling-based metrology. [e] Thermally annealed at 150 °C for 30 min under nitrogen.

separation of the IDTBT:SEBS blend occurred, which resulted in large isolated IDTBT domains, deterring the charge transport efficiency and mechanical deformation of the films. In contrast, the utilization of low-bp such as CF could effectively prevent the large-scale phase separation and promote the formation of a fiber network through the nanoconfinement effect in blend films. This effect enables us to achieve a stretchable film with a low elastic modulus of 72 MPa, large crack at a strain value of 326%, and negligible loss of mobility ($\mu_{h\parallel}^{FET}$ = 0.72 $cm^2 V^{-1} s^{-1}$) at 100% strain. It is envisaged that the molecular aggregation dynamics plays a critical role in the agglomeration and phase separation in conjugated polymer:elastomer blends, which offers an alternative strategy to manipulate the film morphology for a synergistic improvement in the mechanical and electrical properties of stretchable conjugated polymer films.

Nanoconfinement as the basis for the synergistic effect in semiconducting polymer (SP):insulating polymer (IP) blend systems is defined as the confinement of a material in a nanoscale region, which can cause changes in the physical properties of polymers due to interfacial and finite-size effects.[33] Several studies have reported that this confinement can result in a reduction in mechanical properties, glass transition temperature,[137] and elastic modulus,[138] increased crystalline ordering,[139] and better charge transport mobility.[131] Therefore, clarifying the confinement effect of SPs and devising an effective strategy are necessary to design polymer blend composites with multi-aptitudes. Park *et al.* systematically investigated the confinement effect depending on the type of intermolecular interaction of SPs (such as P3HT, P18, DPP2T, 29-DPP, and PCDPTP) in the IP of polystyrene (PS) (Fig. 10c).[140] Based on the correlation between the morphological and charge transport properties on various types of SP:IP blend films, it was found that the 29-DPP-type SP exhibited an improvement in field-effect hole mobilities by 3–4 times (maximum μ_h^{FET} approaching 10 $cm^2 V^{-1} s^{-1}$ for 60DPP:40PS blended type). The combination of temperature-dependent charge carrier mobility analysis and grazing incident-wide angle X-ray spectroscopy (GIWAXS) indicated that the nanostructure of confined SPs exhibited a straight edge-on stacking structure in the blends. According to the above discussion, the capabilities of the blending method to aptly tune the electrical and mechanical properties in an easy and facile manner, coupled with its unsophisticated processing parameters (*e.g.*, blending ratio, molecular weight, and solvent), have created new avenues for many researchers to develop innovative optically transparent, stretchable, and self-healable semiconducting polymer systems for use in TFT devices.

3. Advancement from non-autonomous healing toward autonomous self-healing semiconducting polymers

According to the numerous strategic options previously reported, developing intrinsically stretchable semiconducting polymers through the insertion of bulky soft side chains or *via*

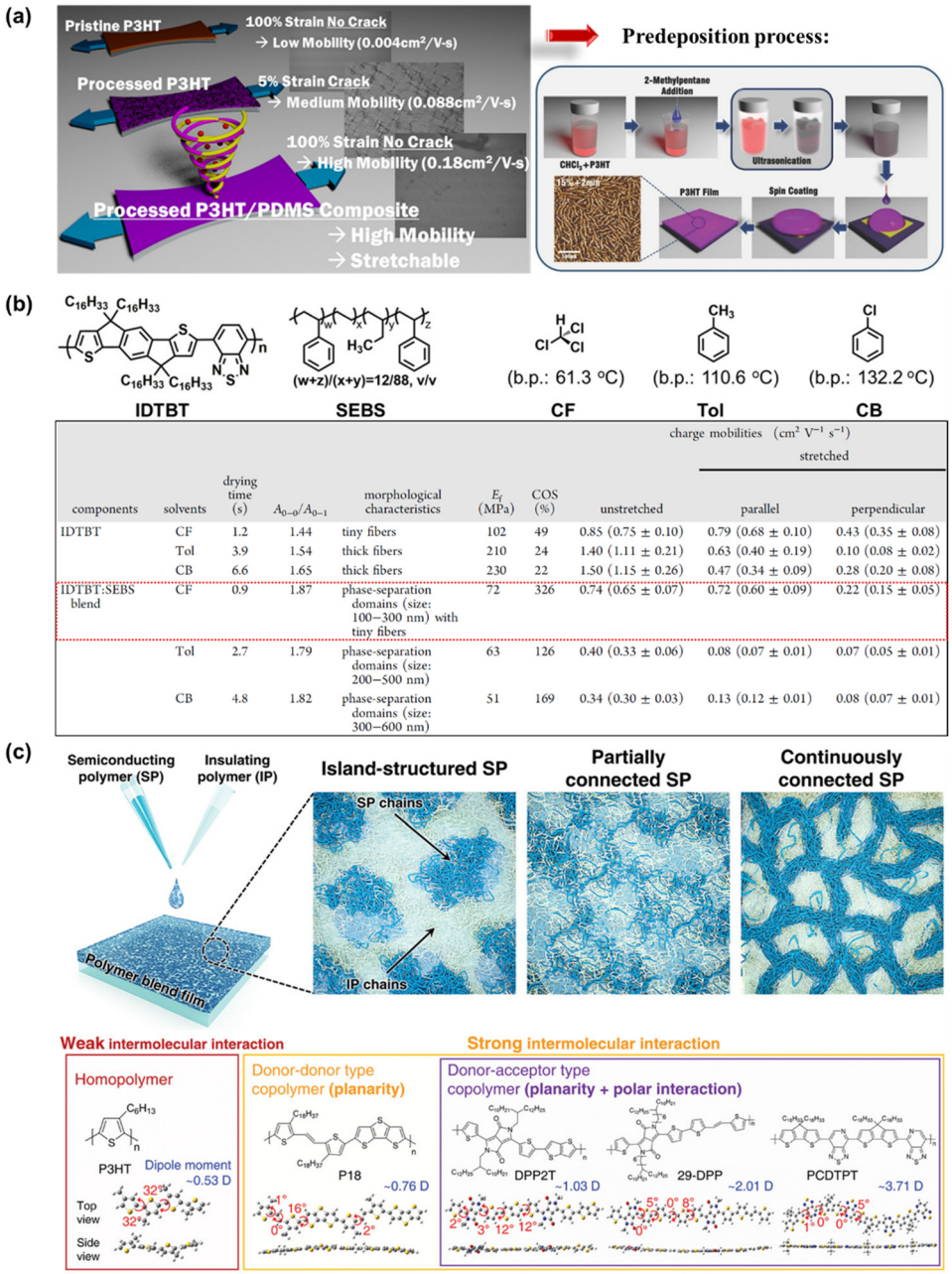

charge mobilities ($cm^2 V^{-1} s^{-1}$)

components	solvents	drying time (s)	A_{0-0}/A_{0-1}	morphological characteristics	E_f (MPa)	COS (%)	unstretched	stretched: parallel	stretched: perpendicular
IDTBT	CF	1.2	1.44	tiny fibers	102	49	0.85 (0.75 ± 0.10)	0.79 (0.68 ± 0.10)	0.43 (0.35 ± 0.08)
	Tol	3.9	1.54	thick fibers	210	24	1.40 (1.11 ± 0.21)	0.63 (0.40 ± 0.19)	0.10 (0.08 ± 0.02)
	CB	6.6	1.65	thick fibers	230	22	1.50 (1.15 ± 0.26)	0.47 (0.34 ± 0.09)	0.28 (0.20 ± 0.08)
IDTBT:SEBS blend	CF	0.9	1.87	phase-separation domains (size: 100–300 nm) with tiny fibers	72	326	0.74 (0.65 ± 0.07)	0.72 (0.60 ± 0.09)	0.22 (0.15 ± 0.05)
	Tol	2.7	1.79	phase-separation domains (size: 200–500 nm)	63	126	0.40 (0.33 ± 0.06)	0.08 (0.07 ± 0.01)	0.07 (0.05 ± 0.01)
	CB	4.8	1.82	phase-separation domains (size: 300–600 nm)	51	169	0.34 (0.30 ± 0.03)	0.13 (0.12 ± 0.01)	0.08 (0.07 ± 0.01)

Fig. 10 (a) Schematic depicting the processed P3HT:PDMS, affording a blended semiconducting film that exhibits superior ductility and notable mobility *versus* the single-component polymer semiconductor counterpart.[73] Copyright: 2016, the American Chemical Society. Schematic illustration of the pre-deposition process.[133] Copyright: 2015, Wiley. (b) Molecular structures of the conjugated polymer IDTBT, elastomer SEBS, and the effect of different deposition treatments on the electrical and mechanical properties of IDTBT and IDTBT:SEBS blend.[136] Copyright: 2022, the American Chemical Society. (c) Representative structural morphologies of SP:IP blend and the DFT-optimized molecular models.[140] Copyright: 2021, Wiley.

the utilization of conjugation breaking units seems to be the preferred approach to generate materials with an increased amorphous content, reduced crystallinity, and improved resistance to mechanical failure, while maintaining good charge transport properties. As reported by Mei *et al.*, CBS can successfully reduce the backbone rigidity, and coupled with the fact that the incorporated CBS is capable of forming weak and reversible intra- and inter-chain bonds, the resulting polymer can be stretched excellently.[26] Furthermore, Zheng *et al.* realized that the incorporation of H-bonding units in DPP-based conjugated polymers is a compelling manner to regulate their crystalline behaviors and mechanical properties.[94] Undoubtedly, these bonds becomes the most common and accessible types of supramolecular interactions to be implemented in π-conjugated polymeric systems. This type of non-covalent interaction is spontaneous, highly dynamic, and can be achieved through a wide variety of functional groups (amide, urea, urethane, carbonate, *etc.*), implying the versatility of the

Table 2 Mechanical and electrical properties of semiconducting polymer-*blended*-PDMS films as determined using a bottom-gate/bottom-contact organic field-effect transistor device

Semiconductors			Mobility ($cm^2 V^{-1} s^{-1}$)			Mechanical properties		
Type	Material	f_{semi} (wt%)	Original	Parallel at 100% strain	Perpendicular at 100% strain	Crack onset strain (%)	Elongation break (%)	Ref.
p	P3HT	100	$\sim 2.3 \times 10^{-3}$	$\sim 1 \times 10^{-5}$	$\sim 2.2 \times 10^{-4}$	25	50	187
p	P3HT/PDMS	5	$\sim 1.8 \times 10^{-3}$	$\sim 1.2 \times 10^{-4}$	$\sim 2.3 \times 10^{-5}$	>100	>100	
p	P3HT/PDMS	0.49	0.17 ± 0.03	0.15 ± 0.01	—	—	182.1 ± 8.6	134
p	P3HT	100	0.02 ± 0.01	0.006 ± 0.001	—	32.6 ± 4.8	—	
p	DPP-DTT/PDMS	0.83	1.53 ± 0.22	1.35 ± 0.04	—	—	140.2 ± 10.2	
p	DPP-DTT	100	0.81 ± 0.11	0.18 ± 0.01	—	20.7 ± 5.2	—	
n	DPPDPyBT/PDMS	0.62	1.25 ± 0.09	1.08 ± 0.02	—	—	133.5 ± 7.6	
n	DPPDPyBT	100	0.43 ± 0.14	0.12 ± 0.01	—	22.5 ± 4.5	—	
p	Homo-P3HT NW	100	$(1.30 \pm 0.4) \times 10^{-2}$	$(1.70 \pm 0.9) \times 10^{-5}$	—	50	10	135
p	P3HT NW/PDMS	10	$(7.85 \pm 2.8) \times 10^{-3}$	$(3.74 \pm 0.7) \times 10^{-4}$	—	—	—	
p	Pristine P3HT	0.75	0.004 ± 0.0005	—	—	>120	—	73
p	Processed P3HT	0.75	0.18 ± 0.03	—	—	> 100	—	
p	Processed P3HT/PDMS composite	0.75	0.11 ± 0.016	—	—	> 100	—	

noncovalent interaction-based synthetic method. Molecular self-healing is another innovative property achieved through the utilization of dynamic H-bonds.

Although the stretchability of polymers has been enhanced, damage due to the forces of stretching, extrusion, and twisting during cumulative use can still occur after long-term repeated operations. By mimicking the self-healing functionality of human skin, artificial self-healing in new smart materials has become a broad concept that covers a wide variety of properties.[141] This phenomenon is also often referred to as self-mending or self-repairing characteristics, which is defined as the ability of a material to partially or fully regain its original material properties upon damage. This particular property possesses the ability to be easily damaged and autonomously recover, which can be found in materials containing dynamic covalent or non-covalent bonds.[142,143] Hydrogen bonds, π–π interactions, metal-ligand bonds, ionic bonds, host–guest complexes, and hydrophobic interactions are the interactions found in non-covalent bonds,[144–151] while Schiff base interactions, Diels–Alder interactions, and borate-ester and disulfide bonds are included in the common dynamic covalent bonds.[152–156] In addition to the bond interactions, the physical molecular diffusion also plays a crucial part in determining the healing rate and characteristics of the damaged polymer surface.[157–160] The diffusion parameters include the chemical characteristics, the chain length, polydispersity indices, and the mechanical properties of the polymer. In some cases, a non-autonomous healing initiating agent and thermal treatment may be needed to trigger self-healing, which are readily available in the form of capsules released upon cracking of the host materials.[161,162]

Considering two important features, *i.e.*, the diffusion of polymer chains and the reformation of broken dynamic bonds,[160] a low glass transition temperature, which promotes polymer chain movement and abundant sites for dynamic interactions, is an implicit requirement in typical intrinsically self-healing semiconducting polymer systems. Since 2001, the Web of Science has listed more than 6000 publications covering the field of self-healing materials;[163] however, only a few studies have reported the successful integration of stretchable conjugated polymers bearing healing capability in TFT devices.[23,24,164–166] This limitation is due to the challenges of fabricating self-healing semiconductor layers, while maintaining good electrical properties. Given that the semiconducting layer for most devices is typically very thin, *i.e.*, < 100 nm, it is difficult to align the damaged areas properly for full healing. This case also applies to the development of stretchable and self-healing materials based on conductive polymers (*e.g.*, poly3,4-ethylene dioxythiophene (PEDOT), polypyrrole (PPy), and polyaniline (PANI)) for feasible applications based on organic electrochemical transistors devices (*e.g.*, bioelectronics and wearable electronics). Other interesting topics related to conducting polymers not covered in this section can be found in recently published reports and reviews.[167–173]

To the best of our knowledge, Bao's group was the first to successfully fabricate magnificent intrinsically stretchable and self-healable semiconducting polymers in TFT devices by utilizing hydrogen-bonding moieties,[23] wherein the nano-size cracks formed by external mechanical stress were found to heal with the assistance of solvent vapour and thermal annealing. The design concept applied was through a backbone engineering approach by synthesizing and incorporating a non-covalent crosslinking moiety of 2,3-pyridine dicarboxamide (PDCA) as a conjugation-break spacer in DPP-based conjugated polymers, namely P(DPP-TVT-X).[23] The design rationale for this intrinsically stretchable polymer was as follows: (1) the H-bonds between the non-conjugated PDCA moieties are moderate, which facilitate stress-energy dissipation during stretching, thus allowing the breaking/reforming of hydrogen bonds when strain is applied; (2) the PDCA moiety containing two amide groups markedly lowers the tensile modulus of the resulting polymer and (3) the charge transport mobility can be well-sustained due to the small loading fraction of PDCA moieties. The combination of the polymer with a small amount of 10 mol% PDCA moiety (P3) could reduce the elastic modulus from

1 GPa to 0.25 GPa without sacrificing the charge mobility compared to the pristine p(DPP-TVT)(P1). As shown in Fig. 11a, the μ_h^{FET} of the P3 thin-film reached up to 1.3 $cm^2\ V^{-1}\ s^{-1}$, and remarkably it could be maintained as high as 1.12 $cm^2\ V^{-1}\ s^{-1}$ even with 100% elongation after a hundred cycles along the direction perpendicular to the strain. On the contrary, pristine P1 failed to maintain its mobility level under 100% applied strain, resulting in a rapid decline to $<10^{-2}$ $cm^2\ V^{-1}\ s^{-1}$. A reference conjugated polymer of P(DPP-TVT-10 mol% Me-PDCA) (P7) with the exclusion of amide-based H-bonding induced by the additional Me-PDCA chain breaker was studied. The distinct influence in mechanical behavior (25% of crack formation strain) of P7 indicates the important contribution of dynamic bonding as a sacrificial bond in the amorphous domain of these systems. Moreover, the mobility of the damaged P3 could be almost fully recovered from 2.4 × 10^{-3} $cm^2\ V^{-1}\ s^{-1}$ to 1.13 $cm^2\ V^{-1}\ s^{-1}$ using a solvent/thermal healing treatment to promote the polymer chain movement. The existence of healing ability in P3 was also proven by AFM characterization, showing that the nano-cracks became less noticeable after thermal treatment.

Besides the PDCA unit, other amine-containing outermost side chains were also developed and investigated. Ocheje *et al.* confirmed the strong influence between the crystallinity, electrical, and mechanical performances of DPP-TVT derivatives with amide-containing alkyl side chains (Fig. 11b).[164] Indeed, the inclusion of 10% amide-containing alkyl side chains (P3) significantly promoted their stretching ability up to 75%, reduced their elastic modulus from 203 MPa to 115 MPa, and facilitated molecular alignment after stretching. Upon stretched

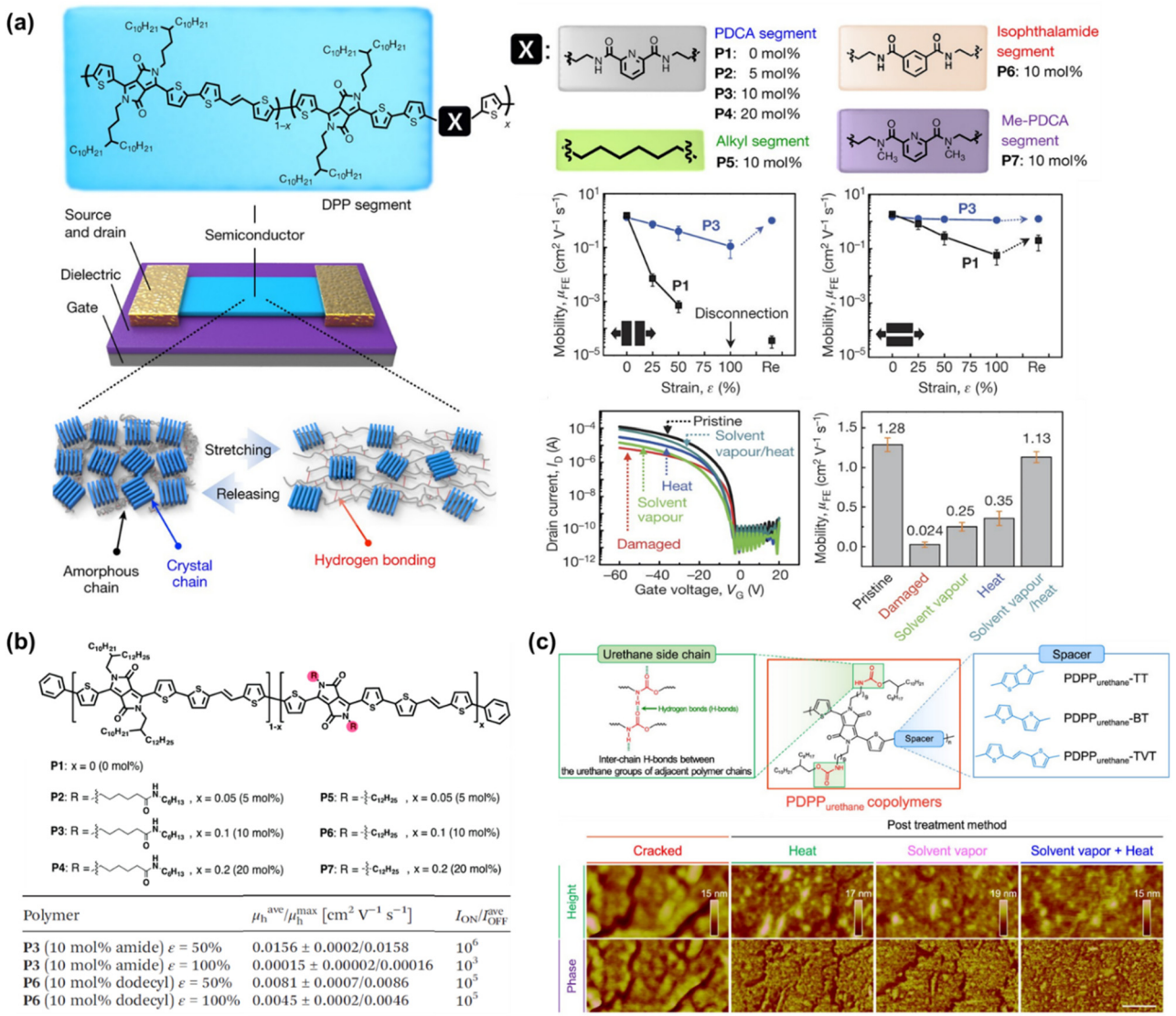

Fig. 11 Modulation and influence of the self-healing properties of conjugated polymers based on dynamic hydrogen bonding. (a) DPP-based polymer with various non-conjugated segments.[23] Copyright: 2016, Springer Nature. (b) Amide-containing alkyl chains in DPP-based conjugated polymers.[164] Copyright: 2018, The Royal Society of Chemistry. (c) Series of DPP-based "alternating" copolymers containing urethane side chains with different donor counterpart co-monomers, denoted as PDPP$_{urethane}$-TT, -BT, and -TVT.[24] Copyright: 2021, Wiley-VCH.

the polymer at 50% toward 100% strain elongation, the polymer suffered from a 2-fold loss in charge mobility, but P3 showed better charge mobility when stretched at 50% strain in comparison to the reference polymer P6, leading to mobility values one order of magnitude higher for P3 than P6. Taking advantage of the H-bond moiety by side-chain engineering, these polymer thin films can heal through proper treatment. For example, solvent vapour (chlorobenzene, 40 °C for 10 min) and thermal annealing (150 °C for 30 min) were needed to promote the chain mobility and molecular rearrangements. Owing to the easy optimization of the performances of TFTs through typical molecular engineering implemented with OH-bonds, the same group probed the impact of the noncovalent interaction orientation (intramolecular and intermolecular H-bonding) on the physical, optoelectronic, and solid-state properties of novel DPP-conjugated polymers.[20] Through a series of detailed characterizations including optical spectroscopy, grazing incidence wide-angle X-ray scattering, and solution small-angle neutron scattering, it was concluded that intramolecular hydrogen bonds were generated in the materials with improved crystallinity and higher effective conjugation in the solid-state.

Similarly, Lee *et al.* synthesized a series of DPP-based "alternating" copolymers containing urethane side chains with different donor co-monomer counterparts, denoted as $PDPP_{urethane}$-TT, -BT, and -TVT.[24] This system featured a well-defined alternating D–A backbone and long-branched urethane side chains capable of providing structural regularity with moderate H-bonding and sufficient solubility. The $PDPP_{urethane}$ derivative spacer exhibited the maximum μ_h^{FET} of 2.58×10^{-2}, 3.46×10^{-2}, and 3.90×10^{-2} $cm^2\ V^{-1}\ s^{-1}$ for $PDPP_{urethane}$-TT, -BT, and -TVT, respectively. The $PDPP_{urethane}$-TVT thin films provided the highest mechanical stability, maintaining their electrical and molecular packing properties up to 100% strain. The typical tensile moduli of DPP-based copolymers are reported to range from 0.1 to 1.0 GPa, whereas $PDPP_{urethane}$-TVT showed much a lower tensile modulus of 0.048 GPa, implying its superior film deformability and ductility. Owing to its superior electrical and mechanical behavior, the healing feature of $PDPP_{urethane}$-TVT based on various post-treatments (*i.e.*, heat, solvent vapor, and solvent vapor + heat) was further investigated *via* AFM analysis. The combination of thermal and solvent vapor provided the most effective healing treatment, as evidenced by the AFM image in Fig. 11c, showing the smooth surface of the thin film after healing. In the case of mild heating and solvent vapor treatment, there were still apparent cracks observed in the AFM image, inferring the poor healing ability, which can plausibly be due to the highly crystalline nature and high glass transition temperature of DPP-based polymers.[174]

Fundamentally different from the reported IP/SP blends, in which macroscopic phase segregation is often involved, Zhao *et al.* proposed a general strategy to fabricate self-healing melt-processable semiconductors (Fig. 12a).[175] The complementary semiconducting polymer blends were composed of flexible DPP-C5 conjugation-break spacer as a matrix polymer due to its low melting temperature (138 °C) and a fully conjugated polymer (DPP-C0) as a tie chain. After the blend of 95 wt% DPP-C5 and 5 wt% DPP-C0 was melt-processed, the resultant average electrical mobility was reported to be 0.4 $cm^2\ V^{-1}\ s^{-1}$ and the current on/off ratios were higher than 10^5 A. With the same combined weight ratio of blended semiconducting polymer, a self-healing test under a melt-processed bottom-gate bottom-contact TFT device was fabricated. It was reported that the initial mobility was 0.29 $cm^2\ V^{-1}\ s^{-1}$ at room temperature, and when the semiconducting layer was fully separated into two parts, the source-drain current dropped to $\approx 10^{-12}$ A, a level similar to the off current level of the device. The semiconducting layer was partially healed at 160 °C for 2 min, indicating rapid healing ability. Then, it only took 30 min to completely heal and the recovered charge mobility was 0.26 $cm^2\ V^{-1}\ s^{-1}$. The authors also succeeded in employing this method for functional semiconductor polymers, where most high-performance semiconducting polymers cannot be liquefied to flow. This, this method overcome the problems associated with the solution processing method.

Inspired by previous work on self-healing and highly stretchable elastomers *via* advanced metal-ligand dynamic interactions,[165] Oh *et al.* fabricated a skin-like semiconducting film through physical blending of a polymer semiconductor and a self-healable elastomer, both of which were dynamically cross-linked by metal coordination (Fig. 12b).[31] In particular, poly(3,6-di(thiophen-2-yl)diketopyrrolo[3,4-*c*]pyrrole-1,4-dione-*alt*-1,2-dithienylethene) with 10 mol% 2,6-pyridinedicarboxamine moieties (DPP-TVT-PDCA) was utilized as the semiconducting material due to its great charge carrier mobility ($>1\ cm^2\ V^{-1}\ s^{-1}$),[23] and poly(dimethylsiloxane-*alt*-2,6-pyridinedicarbozamine) with an Fe(III) ion (PDMS-PDCA-Fe elastomer) as the insulating, stretchable, and healable polymer.[165] The multiple dynamic coordinate covalent bonds with three different bonding strengths ($Fe–N_{pyridyl}$, strong; $Fe–N_{amido}$, medium; and $Fe–O_{amido}$, weak) facilitated the dynamic cross-linking for high stretchability (fracture strain >1300%) and the material could be fully self-healed at room temperature within 1 day. Furthermore, the values of the field-effect mobility evaluated in a bottom-contact bottom-gate-structured TFT on a healed semiconducting film was recovered from the initial mobility value before fracture of 4.7×10^{-3} $cm^2\ V^{-1}\ s^{-1}$ to 2.8×10^{-3} $cm^2\ V^{-1}\ s^{-1}$. These results indicate that the practical application of self-healable TFT devices at room temperature without any external stimuli is one-step closer to being achieved, where this behavior is called "autonomous self-healing". Furthermore, this semiconducting layer has been successfully implemented in the innovative development of fully stretchable active-matrix sensor-based e-skin.

Recently, Zhang *et al.* also used physical blending to manufacture new self-healing semiconducting composites, but the mechanism of self-healing was different from previous reports.[166] Taking advantage of butyl rubber (BR) as the elastomer with outstanding elasticity (a low persistence length of 5.2 Å), strong adhesion, and excellent barrier properties to both oxygen and water, together with PDPPTVT as a p-type donor–acceptor semiconducting polymer with high charge transport mobility,[174] these two well-known materials were blended. A free-standing tensile tester was used to evaluate the mechanical and self-healing behavior in various blend ratios between

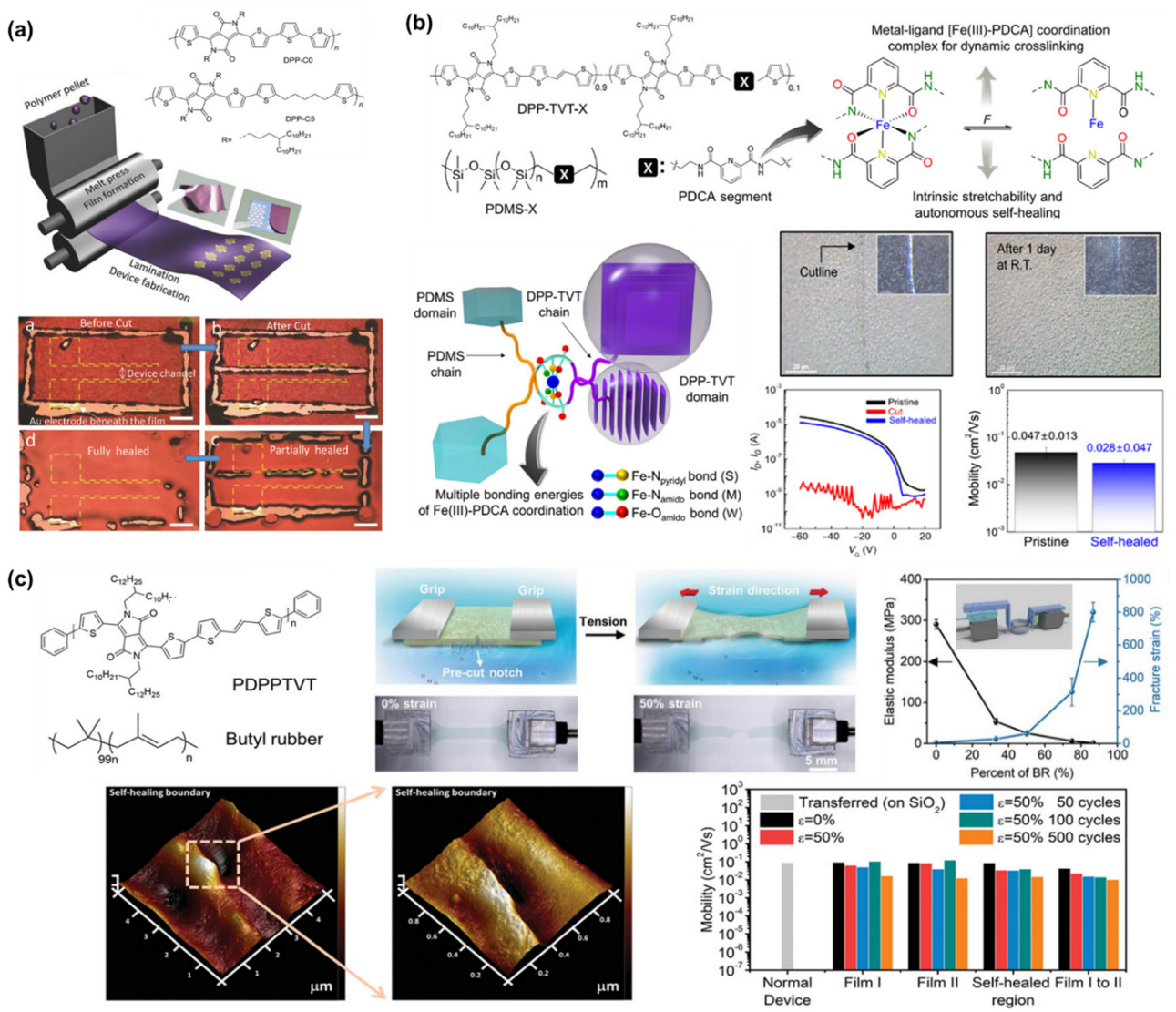

Fig. 12 Stretchable and self-healable semiconducting polymer *via* blending strategy. (a) Materials, fabrication procedure, and TFT characterization of melt-processing of complementary self-healable semiconducting polymer blends.[175] Copyright: 2017, Wiley. (b) Illustration and the mechanical-electrical properties of Fe(III)-PDCA ligand bonding of PDMS-PDCA and DPP-TVT-PDCA in the blend film.[31] Copyright: 2019, Science Advances. (c) 3D-schematic illustration, optical images of notched film before and after tensile deformation on water surface, and the self-healing test as a function on electrical performances of 2 : 3 PDPPTVT/BR film.[166] Copyright: 2020, Wiley.

PDPPTVT and BR (Fig. 12c). As the weight fraction of BR increased to ~90%, the semiconducting polymer composite showed a significant drop in elastic modulus to 1 MPa and great improvement in fracture strain exceeding 800%. Given that the BR polymer endows tackiness and fast segmental motion to low T_g BR polymer chains at room temperature,[174,176] the polymer chains that reconstructed during contact led to autonomous self-healing within a few seconds at room temperature, and the film could be stretched up to 150% of its original length after healing. As is the case with electronic performance, the charge mobility was maintained on the same order of magnitude, even after 500 stretch-release cycles at 50% strain. Additionally, this new composite exhibited outstanding tear-resistant properties, which were attributed to the highly entangled BR network being able to redistribute stress, thus preventing crack propagation and increasing the durability. From a mechanical perspective, this material successfully displayed the lowest modulus and the highest deformability compared to other polymer designs.[33,77,81,104,177–181] Overall, these tear-resistant and room temperature self-healable semiconducting polymers feature special functionalities, which can facilitate future developments for wearable applications.

4. Perspectives

As has been elucidated from the previous sections, the presence of self-healing ability in semiconducting polymers is mainly

derived from the dynamic covalent and non-covalent interaction found in a variety of bond formations.[142,143] However, this perspective focuses on the stretchable and self-healable semiconducting polymers that are scarce and less well-exploited in TFTs due to the limitations and challenges associated with this emerging technology. Recent advances in the performance of conjugated polymers through molecular design or physical blending have successfully exhibited field-effect mobilities >1 cm^2 V^{-1} s^{-1},[23,166] similar to the electrical performance of amorphous silicon thin-film transistors.[182–184] Furthermore, after integrating self-healable semiconducting polymers in TFT devices, they can withstand extreme mechanical behavior. However, to actualize a complete set of self-healable TFTs, three self-healable components need to be developed concurrently, *i.e.*, semiconductors, dielectrics, and three-terminal electrodes. Compared to the fabrication of self-healable semiconducting polymers, the development of other self-healable components in TFTs is simpler and has met the standards for implementation in TFTs to be integrated into sensors, memory devices, and drive circuits for displays.[106,149,165,185,186] For example, in 2016, Bao and co-workers introduced the design of electrically stable and self-healable dielectric layers based on metal-ligand coordination interaction in a PDMS matrix.[149] The supramolecular non-covalent bond contained in this interaction allows impeccable self-healing property for potential applications in wearable sensors and electronic skins. Through the proper selection of counter anions, TFTs with hysteresis-free transfer characteristics can be generated. Self-healable conductive materials composed of a 3D percolation network of carbon nanotubes (CNTs) or silver nanowires (AgNWs) embedded in a self-healable polymer matrix were used as source, drain, and gate components to fabricate a fully stretchable and self-healable multi-functional electronic skin system.[185] This unique property was achieved by taking advantage of the low glass transition temperature and dynamic hydrogen bonding properties of an elegant elastomeric matrix,[160] where the broken conductive network present in the non-covalently bonded hydrogen moieties could be autonomously recovered from disconnection during the self-healing process.

Continuing the discussion in Section 3, the same group succeeded in fabricating (DPP-TVT-PDCA)-*blended*-(PDMS-PDCA-Fe elastomer) as a stretchable and self-healable semiconducting polymer film for an active-matrix strain-sensing array.[31] The Fe(III)-PDCA coordination complex inside the polymer blend was comprised of 3 types of bonding forces (Fe–$N_{pyridyl}$, strong; Fe–N_{amido}, medium; and Fe–O_{amido}, weak), which could facilitate the crosslinking process for self-healing capability based on non-covalent interaction. Fig. 13 shows that a fully stretchable 5 × 5 active-matrix sensor-based e-skin was capable of detecting pressure-induced deformation, with the simultaneous visualization of the applied strain. The active area of each pixel has a channel width of 1 mm and channel length of 150 μm. All devices showed good uniformity with a maximum mobility of 0.11 cm^2 V^{-1} s^{-1} and an average mobility of 0.076 ± 0.019 cm^2 V^{-1} s^{-1}. It needs to be emphasized that the authors inserted a self-healing semiconducting film between stretchable sandwich layers. Thus, to construct

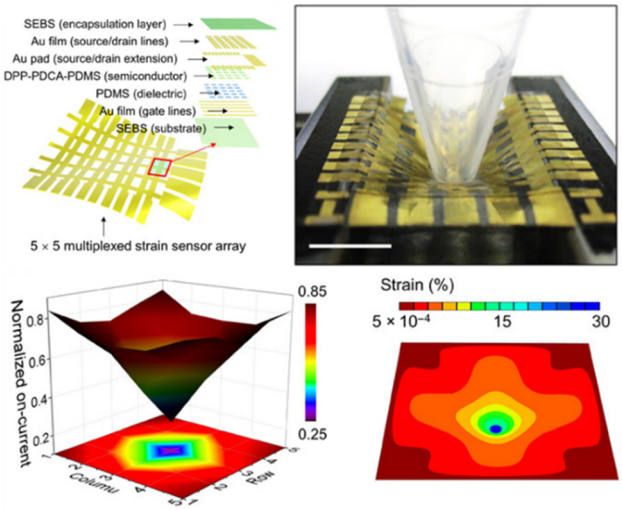

Fig. 13 Architecture, photograph, normalized on-current, and simulation results of strain applied by poking with a plastic bar to the fully stretchable active-matrix TFT array containing self-healable semiconducting polymer.[31] Copyright: 2019, Science Advances.

skin-like sensory devices and verifiably operate within a medically safe voltage range, integration with self-healable conductors and especially high-k dielectric materials still needs to be developed.

Despite the very promising advances in the manufacture of autonomous self-healable semiconducting polymers, their implementation in real applications or commercial products is still in its infancy. To date, the application of self-healing materials in devices is still at the proof-of-concept stage. Besides the possible mismatch between self-healing ability and electrical mobility, the application of self-healable semiconducting polymers in TFT devices is currently limited due to their tedious fabrication process, which may be incompatible with existing electronic technologies established in the silicon industry. Technically, how to make them comparable in size so they can fit in the architecture of boards, especially on ultra-thin semiconductor films at the micro- and nano-scale needs to be considered. Therefore, scalable and reliable fabrication processes such as patterning or printing should be developed for the mass production of self-healing devices and electronics. It should be noted that the self-healing process remains relatively slow and the utilization of self-healing has thus far been limited to small-area damage (nano crack), and thus self-healing capabilities at damage scales larger than layer thickness, which are rapid, repeatable, and autonomous should be explored further. Lastly, the current electronic properties are not yet comparable between non-healable electronic devices and healable functional electronic devices. Thus, further perseverance in the field of new design concepts for self-healable semiconducting polymers is required.

5. Conclusions

This review presented an update on the current status and developments of stretchable to self-healing semiconducting

polymers in TFT devices. In the early stages of research, the engineering strategy focused on the fundamental morphological properties of the semiconducting polymer itself such as MW and RRe, and thus other considerations during the preparation of thin films was thoroughly reviewed. As an example, polythiophene derivatives having a high MW possess a superior synergistic relationship between mobility-stretchability properties. An enhanced chain entanglement effect and greater connectivity between crystallites in P3HT and self-aggregation of polymer chains are the advantages of utilizing high MW polymers. The main part of this report, before moving on to autonomous healing properties integrated in TFT devices, elaborated and discussed the seven main approaches and additional function compounds used to overcome the compromise between electrical-mechanical properties. Based on the range of limitations of this review, only the molecular spacer and symmetric side-chain approaches could achieve a field-effect mobility of >1 cm^2 V^{-1} s^{-1} even in the stretched state up to 100%, together with a lower elastic modulus (<0.1 GPa), indicating excellent deformability and ductility to promote tolerance toward their electrical functionalities under repeated mechanical loading-unloading cycles over long-term usage. The complementary part of this report linked the chosen approaches for designing novel intrinsically stretchable semiconducting polymers with partial or full healing ability implemented with the polymers used in device technologies. Hence, the structural diversity of D–A type polymers has been well selected for the more innovative design of non-covalent interaction-induced self-healing capability. Given that most intrinsically self-healable semiconducting polymers are constructed *via* complex engineering strategies, the conjugated polymer blending approach was introduced as a modest method with fruitful advantages. This method results in autonomous self-healing capability and a remarkable enhancement in mechanical adherence for high-mobility polymer semiconductors in an easy and facile manner.

Author contributions

Y.-C. C. conceived the main concept of the review article. L. L. organized the overall manuscript and wrote the introduction, and the parts relating to fundamental properties of polythiophene derivatives, backbone-engineering approaches, the advances from non-autonomous to autonomous self-healing semiconducting polymers, perspectives and conclusions in the manuscript. A. N. wrote the parts relating to the solution processing and fabrication effect, structural engineering of polymer side chains, and preparing the summary table. S. P. P. organized the overall manuscript. The manuscript was written through contributions from all the authors. All the authors have given approval to the final version of the manuscript.

Conflicts of interest

There are no conflicts to declare.

Acknowledgements

Y.-C. C. is thankful for financial support from the Ministry of Science and Technology in Taiwan (MOST 110-2221-E-011-009).

Notes and references

1 T. Ito, H. Shirakawa and S. Ikeda, *J. Polym. Sci., Polym. Chem. Ed.*, 1975, **13**, 1943–1950.
2 A. J. Heeger, *J. Phys. Chem. B*, 2001, **105**, 8476–8491.
3 H. Shirakawa, E. J. Louis, A. G. Macdiarmid, C. K. Chiang and A. J. Heeger, *J. Chem. Soc., Chem. Commun.*, 1977, 578–580.
4 R. M. Pankow and B. C. Thompson, *Polymer*, 2020, **207**, 122874.
5 E. J. Markvicka, M. D. Bartlett, X. Huang and C. Majidi, *Nat. Mater.*, 2018, **17**, 618–624.
6 Y. Liu, M. Pharr and G. A. Salvatore, *ACS Nano*, 2017, **11**, 9614–9635.
7 S. Wang, J. Y. Oh, J. Xu, H. Tran and Z. Bao, *Acc. Chem. Res.*, 2018, **51**, 1033–1045.
8 I. You, D. G. Mackanic, N. Matsuhisa, J. Kang, J. Kwon, L. Beker, J. Mun, W. Suh, T. Y. Kim, Z. Bao and U. Jeong, *Science*, 2020, **370**, 961–965.
9 T. Huynh, P. Sonar and H. Haick, *Adv. Mater.*, 2017, **29**, 1604973.
10 Z. Zhang, W. Wang, Y. Jiang, Y. X. Wang, Y. Wu, J. C. Lai, S. Niu, C. Xu, C. C. Shih, C. Wang, H. Yan, L. Galuska, N. Prine, H. C. Wu, D. Zhong, G. Chen, N. Matsuhisa, Y. Zheng, Z. Yu, Y. Wang, R. Dauskardt, X. Gu, J. B. H. Tok and Z. Bao, *Nature*, 2022, **603**, 624–630.
11 H. Tien, Y. Huang, Y. Chiu, Y.-H. Cheng, C.-C. Chueh and W.-Y. Lee, *J. Mater. Chem. C*, 2021, **9**, 2660–2684.
12 Y. W. Huang, Y. C. Lin, H. C. Yen, C. K. Chen, W. Y. Lee, W. C. Chen and C. C. Chueh, *Chem. Mater.*, 2020, **32**, 7370–7382.
13 T. Someya, Z. Bao and G. G. Malliaras, *Nature*, 2016, **540**, 379–385.
14 S. Lage-rivera, A. Ares-pernas and M. Abad, *Int. J. Energy Res.*, 2022, 1–24.
15 D. H. Cho, K. G. Cho, S. An, M. S. Kim, H. W. Oh, J. Yeo, W. C. Yoo, K. Hong, M. Kim and K. H. Lee, *Energy Storage Mater.*, 2022, **45**, 323–331.
16 J. Kang, J. B. Tok and Z. Bao, *Nat. Electron.*, 2019, **2**, 144–150.
17 S. E. Root, S. Savagatrup, A. D. Printz, D. Rodriquez and D. J. Lipomi, *Chem. Rev.*, 2017, **117**, 6467–6499.
18 S. Holliday, J. E. Donaghey and I. McCulloch, *Chem. Mater.*, 2014, **26**, 647–663.
19 A. Gasperini, G. J. N. Wang, F. Molina-Lopez, H. C. Wu, J. Lopez, J. Xu, S. Luo, D. Zhou, G. Xue, J. B. H. Tok and Z. Bao, *Macromolecules*, 2019, **52**, 2476–2486.
20 M. U. Ocheje, R. B. Goodman, K. T. Lu, Y. Wang, L. A. Galuska, L. Soullard, Z. Cao, S. Zhang, M. Yadiki, X. Gu, Y. C. Chiu and S. Rondeau-Gagné, *Chem. Mater.*, 2021, **33**, 8267–8277.

21 L. A. Galuska, M. U. Ocheje, Z. C. Ahmad, S. Rondeau-Gagné and X. Gu, *Chem. Mater.*, 2022, **34**, 2259–2267.
22 M. U. Ocheje, B. P. Charron, Y. Cheng, C. Chuang, A. Soldera, Y. Chiu and S. Rondeau-gagne, *Macromolecules*, 2018, **51**, 1336–1344.
23 J. Y. Oh, S. Rondeau-Gagné, Y. C. Chiu, A. Chortos, F. Lissel, G. J. N. Wang, B. C. Schroeder, T. Kurosawa, J. Lopez, T. Katsumata, J. Xu, C. Zhu, X. Gu, W. G. Bae, Y. Kim, L. Jin, J. W. Chung, J. B. H. Tok and Z. Bao, *Nature*, 2016, **539**, 411–415.
24 M. Y. Lee, S. Dharmapurikar, S. J. Lee, Y. Cho, C. Yang and J. H. Oh, *Chem. Mater.*, 2020, **32**, 1914–1924.
25 X. Yu, C. Li, C. Gao, X. Zhang, G. Zhang and D. Zhang, *SmartMat*, 2021, **2**, 347–366.
26 Y. Zhao, X. Zhao, Y. Zang, C. Di, Y. Diao and J. Mei, *Macromolecules*, 2015, **48**, 2048–2053.
27 H. J. Cheon, T. K. An and Y. H. Kim, *Macromol. Res.*, 2022, **30**, 71–84.
28 J. Mei, D. H. Kim, A. L. Ayzner, M. F. Toney and Z. Bao, *J. Am. Chem. Soc.*, 2011, **133**, 20130–20133.
29 I. Kang, H. Yun, D. S. Chung, S. Kwon and Y. Kim, *J. Am. Chem. Soc.*, 2013, **135**, 14896–14899.
30 C. Lu, W. Y. Lee, X. Gu, J. Xu, H. H. Chou, H. Yan, Y. C. Chiu, M. He, J. R. Matthews, W. Niu, J. B. H. Tok, M. F. Toney, W. C. Chen and Z. Bao, *Adv. Electron. Mater.*, 2017, **3**, 1600311.
31 J. Y. Oh, D. Son, T. Katsumata, Y. Lee, Y. Kim, J. Lopez, H. C. Wu, J. Kang, J. Park, X. Gu, J. Mun, N. G. J. Wang, Y. Yin, W. Cai, Y. Yun, J. B. H. Tok and Z. Bao, *Sci. Adv.*, 2019, **5**, eaav3097.
32 S. Nikzad, H. Wu, J. Kim, C. M. Mahoney, J. R. Matthews, W. Niu, Y. Li, H. Wang, W. Chen, M. F. Toney, M. He and Z. Bao, *Chem. Mater.*, 2020, **32**, 897–905.
33 J. Xu, S. Wang, G. N. Wang, C. Zhu, S. Luo, L. Jin, X. Gu, S. Chen, V. R. Feig, J. W. F. To, S. Rondeau-gagné, J. Park, B. C. Schroeder, C. Lu, J. Y. Oh, Y. Wang, Y. Kim, H. Yan, R. Sinclair, D. Zhou, G. Xue, B. Murmann, C. Linder, W. Cai, J. B. H. Tok, J. W. Chung and Z. Bao, *Science*, 2017, **64**, 59–64.
34 K. Sim, Z. Rao, F. Ershad and C. Yu, *Adv. Mater.*, 2019, **32**, 1902417.
35 Y. Zheng, S. Zhang, B. Tok and Z. Bao, *J. Am. Chem. Soc.*, 2022, **144**, 4699–4715.
36 Z. Bao, A. Dodabalapur and A. J. Lovinger, *Appl. Phys. Lett.*, 1996, **69**, 4108.
37 K. R. Amundson, B. J. Sapjeta, A. J. Lovinger and Z. Bao, *Thin Solid Films*, 2002, **414**, 143–149.
38 B. H. Yang, T. J. Shin, L. Yang, K. Cho, C. Y. Ryu and Z. Bao, *Adv. Energy Mater.*, 2005, **15**, 671–676.
39 H. Yang, T. A. E. J. O. O. Shin, Z. Bao and C. Y. Ryu, *J. Polym. Sci., Part B: Polym. Phys.*, 2007, **45**, 1303–1312.
40 A. Chortos, J. Lim, J. W. F. To, M. Vosgueritchian, T. J. Dusseault, T. Kim, S. Hwang and Z. Bao, *Adv. Mater.*, 2014, **26**, 4253.
41 B. M. Brinkmann and P. Rannou, *Adv. Funct. Mater.*, 2007, **17**, 101–108.
42 M. Brinkmann, *J. Polym. Sci., Part B: Polym. Phys.*, 2011, **49**, 1218–1233.
43 C. P. Buckley and A. J. Kovacs, *Colloid Polym. Sci.*, 1976, **254**, 695–715.
44 E. Chen, A. J. Jing, X. Weng, P. Huang, S. Lee, S. Z. D. Cheng, B. S. Hsiao and F. Yeh, *Polymer*, 2003, **44**, 6051–6058.
45 S. J. Organ, G. Ungar and A. Keller, *Macromolecules*, 1989, **22**, 1995–2000.
46 E. Mena-osteritz, A. Meyer, B. M. W. Langeveld-voss, R. A. J. Janssen, E. W. Meijer and P. Bäuerle, *Angew. Chem., Int. Ed.*, 2000, **39**, 2679–2684.
47 R. J. Kline, M. D. McGehee, E. N. Kadnikova, J. Liu, J. M. J. Fréchet and M. F. Toney, *Macromolecules*, 2005, **38**, 3312–3319.
48 N. E. Persson, P. H. Chu, M. McBride, M. Grover and E. Reichmanis, *Acc. Chem. Res.*, 2017, **50**, 932–942.
49 B. O'Connor, R. J. Kline, B. R. Conrad, L. J. Richter, D. Gundlach, M. F. Toney and D. M. DeLongchamp, *Adv. Funct. Mater.*, 2011, **21**, 3697–3705.
50 D. Gargi, R. J. Kline, D. M. Delongchamp, D. A. Fischer, M. F. Toney and B. T. O'Connor, *J. Phys. Chem. C*, 2013, **117**, 17421–17428.
51 R. J. Kline, M. D. McGehee, E. N. Kadnikova, J. Liu and J. M. J. Frechet, *Adv. Mater.*, 2003, **15**, 1519–1522.
52 F. Peter, V. Koch, J. Rivnay, S. Foster, C. Müller, J. M. Downing, E. Buchaca-domingo, P. Westacott, L. Yu, M. Yuan, M. Baklar, Z. Fei, C. Luscombe, M. A. Mclachlan, M. Heeney, G. Rumbles, C. Silva, A. Salleo, J. Nelson, P. Smith and N. Stingelin, *Prog. Polym. Sci.*, 2013, **38**, 1978–1989.
53 D. Rodriquez, J. Kim, S. E. Root, Z. Fei, P. Bou, M. Heeney, T. Kim and D. J. Lipomi, *Appl. Mater. Interfaces*, 2017, **9**, 8855–8862.
54 Y. Kim, S. Cook, S. M. Tuladhar, S. A. Choulis, J. Nelson, J. R. Durrant, D. D. C. Bradley, M. Giles, I. Mcculloch, C. Ha and M. Ree, *Nat. Mater.*, 2006, **5**, 197–203.
55 C. H. Woo, B. C. Thompson, B. J. Kim, M. F. Toney and J. M. J. Fre, *J. Am. Chem. Soc.*, 2008, **130**, 16324–16329.
56 H. Sirringhaus, N. Tessler and R. H. Friend, *Science*, 1998, **280**, 1741–1744.
57 H. Sirringhaus, P. J. Brown, R. H. Friend, M. M. Nielsen, K. Bechgaard, B. M. W. Langeveld-Voss, A. J. H. Spiering, R. A. J. Janssen, E. W. Meijer, P. Herwig and D. M. de Leeuw, *Nature*, 1999, **401**, 685–688.
58 J. Kim, J. Kim, W. Lee, H. Yu, H. J. Kim, I. Song, M. Shin, J. H. Oh, U. Jeong, T. Kim and B. J. Kim, *Macromolecules*, 2015, **48**, 4339–4346.
59 H. Park, B. S. Ma, J. Kim, Y. Kim, H. J. Kim, D. Kim, H. Yun, J. Han, F. S. Kim, T. Kim and B. J. Kim, *Macromolecules*, 2019, **52**, 7721–7730.
60 B. O'Connor, E. P. Chan, C. Chan, B. R. Conrad, L. J. Richter, R. J. Kline, M. Heeney, I. McCulloch, C. L. Soles and D. M. DeLongchamp, *ACS Nano*, 2010, **4**, 7538–7544.
61 B. C. Schroeder, Y. Chiu, X. Gu, Y. Zhou, J. Xu, J. Lopez, C. Lu, M. F. Toney and Z. Bao, *Adv. Electron. Mater.*, 2016, **2**, 1600104.

62 Y. D. Park, J. K. Park, J. H. Seo, J. D. Yuen, W. H. Lee, K. Cho and G. C. Bazan, *Adv. Energy Mater.*, 2011, **1**, 63–67.
63 C. Mcdowell, M. Abdelsamie, M. F. Toney and G. C. Bazan, *Adv. Mater.*, 2018, **1707114**, 1–30.
64 N. E. Jackson, K. L. Kohlstedt, B. M. Savoie, O. De Cruz, G. C. Schatz, L. X. Chen and M. A. Ratner, *J. Am. Chem. Soc.*, 2015, **137**, 6254–6262.
65 W. Lee, G. Giri, Y. Diao, C. J. Tassone, J. R. Matthews, M. L. Sorensen, S. C. B. Mannsfeld, W. Chen, H. H. Fong, J. B. Tok, M. F. Toney, M. He and Z. Bao, *Adv. Funct. Mater.*, 2014, **24**, 3524–3534.
66 K. Zhao, X. Yu, R. Li, A. Amassian and Y. Han, *J. Mater. Chem. C*, 2015, **3**, 9842–9848.
67 H. Hu, K. Zhao, N. Fernandes, P. Boufflet, J. H. Bannock, L. Yu, J. C. de Mello, N. Stingelin, M. Heeney, E. P. Giannelis and A. Amassian, *J. Mater. Chem. C*, 2015, **3**, 7394–7404.
68 L. Janasz, D. Chlebosz, M. Gradzka, W. Zajaczkowski, T. Marszalek, K. Mullen, J. Ulanski, A. Kiersnowski and W. Pisula, *J. Mater. Chem. C*, 2016, **4**, 11488–11498.
69 J. Y. Oh, M. Shin, T. Il Lee, W. S. Jang, Y. Min, J. Myoung, H. K. Baik and U. Jeong, *Macromolecules*, 2012, **45**, 7504–7513.
70 H. Liu, C. H. Reccius and H. G. Craighead, *Appl. Phys. Lett.*, 2005, **87**, 253106.
71 Y. Yuan, G. Giri, A. L. Ayzner, A. P. Zoombelt, S. C. B. Mannsfeld, J. Chen, D. Nordlund, M. F. Toney, J. Huang and Z. Bao, *Nat. Commun.*, 2014, **5**, 3005.
72 J. Chen, H. Hsieh, Y. Chiu, W. Lee, C. Hung, C. Chueh and W. Chen, *J. Mater. Chem. C*, 2020, **8**, 873–882.
73 D. Choi, H. Kim, N. Persson, P. Chu, M. Chang, J. Kang, S. Graham and E. Reichmanis, *Chem. Mater.*, 2016, **28**, 1196–1204.
74 R. Noriega, J. Rivnay, K. Vandewal, F. P. V. Koch, N. Stingelin, P. Smith, M. F. Toney and A. Salleo, *Nat. Mater.*, 2013, **12**, 1038–1044.
75 J. S. Ross, S. Wu, H. Yu, N. J. Ghimire, A. M. Jones, G. Aivazian, J. Yan, D. G. Mandrus, D. Xiao, W. Yao and X. Xu, *Nat. Commun.*, 2013, **4**, 1474.
76 D. Venkateshvaran, M. Nikolka, A. Sadhanala, V. Lemaur, M. Zelazny, M. Kepa, M. Hurhangee, A. J. Kronemeijer, V. Pecunia, I. Nasrallah, I. Romanov, K. Broch, I. McCulloch, D. Emin, Y. Olivier, J. Cornil, D. Beljonne and H. Sirringhaus, *Nature*, 2014, **515**, 384–388.
77 C. Müller, S. Goffri, D. W. Breiby, J. W. Andreasen, H. D. Chanzy, R. A. J. Janssen, M. M. Nielsen, C. P. Radano, H. Sirringhaus, P. Smith and N. Stingelin-Stutzmann, *Adv. Funct. Mater.*, 2007, **17**, 2674–2679.
78 J. Chang, B. Sun, D. W. Breiby, M. M. Nielsen, T. I. Sölling, M. Giles, I. Mcculloch and H. Sirringhaus, *Chem. Mater.*, 2004, **16**, 4772–4776.
79 J.-T. Wang, S. Takshima, H.-C. Wu, C.-C. Shih, T. Isono, T. Kakuchi, T. Satoh and W.-C. Chen, *Macromolecules*, 2017, **50**, 1442–1452.
80 Y.-C. Chiang, S. Kobayashi, T. Isono, C.-C. Shih, T. Shingu, C.-C. Hung, H.-C. Hsieh, S.-H. Tung, T. Satoh and W.-C. Chen, *Polym. Chem.*, 2019, **10**, 5452–5464.
81 R. Peng, B. Pang, D. Hu, M. Chen, G. Zhang, X. Wang, H. Lu, K. Cho and L. Qiu, *J. Mater. Chem. C*, 2015, **3**, 3599–3606.
82 T. Higashihara, S. Fukuta, Y. Ochiai, T. Sekine, K. Chino, T. Koganezawa and I. Osaka, *ACS Appl. Polym. Mater.*, 2019, **1**, 315–320.
83 S. Miyane, H. Wen, W. Chen and T. Higashihara, *Polym. Chem.*, 2018, **56**, 1787–1794.
84 M. Funahashi and A. Sonoda, *Org. Electron.*, 2012, **13**, 1633–1640.
85 J. Lee, A. Han, J. Kim, Y. Kim, J. H. Oh and C. Yang, *J. Am. Chem. Soc.*, 2012, **134**, 20713–20721.
86 K. Fujita, Y. Sumino, K. Ide, S. Tamba, K. Shono, J. Shen, T. Nishino, A. Mori and T. Yasuda, *Macromolecular*, 2016, **49**, 1259–1269.
87 J. Shen, K. Fujita, T. Matsumoto, C. Hongo, M. Misaki, K. Ishida, A. Mori and T. Nishino, *Macromol. Chem. Phys.*, 2017, **218**, 1700197.
88 A. Salleo, T. W. Chen and A. R. Völkel, *Phys. Rev. B: Condens. Matter Mater. Phys.*, 2004, **70**, 115311.
89 A. F. Paterson, S. Singh, K. J. Fallon, T. Hodsden, Y. Han, B. C. Schroeder, H. Bronstein, M. Heeney, I. Mcculloch and T. D. Anthopoulos, *Adv. Mater.*, 2018, **1801079**, 1–33.
90 Y. Guan, A. Thukral, S. Zhang, K. Sim, X. Wang, Y. Zhang, Z. R. Faheem Ershad5, F. Pan, P. Wang, J. Xiao and C. Yu, *Sci. Adv.*, 2020, **6**, eabb3656.
91 S. Savagatrup, X. Zhao, E. Chan, J. Mei and D. J. Lipomi, *Macromol. Rapid Commun.*, 2016, **37**, 1623–1628.
92 E. L. Melenbrink, K. M. Hilby, M. A. Alkhadra, S. Samal, D. J. Lipomi and B. C. Thompson, *Appl. Mater. Interfaces*, 2018, **10**, 32426–32434.
93 J. Mun, G. N. Wang, J. Y. Oh, T. Katsumata, F. L. Lee, J. Kang, H. Wu, F. Lissel, S. Rondeau-gagné and J. B. Tok, *Adv. Funct. Mater.*, 2018, **28**, 1804222.
94 Y. Zheng, M. Ashizawa, S. Zhang, J. Kang, S. Nikzad, Z. Yu, Y. Ochiai, C. Wu, H. Tran, J. Mun, Y. Zheng, J. B. Tok, X. Gu and Z. Bao, *Chem. Mater.*, 2020, **32**, 5700–5714.
95 D. Liu, J. Mun, G. Chen, N. J. Schuster, W. Wang, Y. Zheng, S. Nikzad, J. Lai, Y. Wu, D. Zhong, Y. Lin, Y. Lei, Y. Chen, S. Gam, J. W. Chung, Y. Yun, B. Tok and Z. Bao, *J. Am. Chem. Soc.*, 2021, **143**, 11679–11689.
96 K. Shi, W. Zhang, D. Gao, S. Zhang, Z. Lin, Y. Zou, L. Wang and G. Yu, *Adv. Mater.*, 2018, **30**, 1705286.
97 Y. C. Lin, Y. W. Huang, C. C. Hung, Y. C. Chiang, C. K. Chen, L. C. Hsu, C. C. Chueh and W. C. Chen, *ACS Appl. Mater. Interfaces*, 2020, **12**, 50648–50659.
98 J. Mun, Y. Ochiai, W. Wang, Y. Zheng, Y. Zheng, H. Wu, N. Matsuhisa, T. Higashihara, J. B. Tok, Y. Yun and Z. Bao, *Nat. Commun.*, 2021, **12**, 3572.
99 A. D. Printz, S. Savagatrup, D. J. Burke, T. N. Purdy and D. J. Lipomi, *RSC Adv.*, 2014, **4**, 13635–13643.
100 S. Savagatrup, A. D. Printz, D. Rodriquez and D. J. Lipomi, *Macromolecules*, 2014, **47**, 1981–1992.
101 Y. C. Lin, Y. W. Huang, Y. S. Wu, J. S. Li, Y. F. Yang, W. C. Chen and C. C. Chueh, *ACS Appl. Polym. Mater.*, 2021, **3**, 1628–1637.

102 S. Allard, M. Forster, B. Souharce, H. Thiem and U. Scherf, *Angew. Chem., Int. Ed.*, 2008, **47**, 4070–4098.
103 H. F. Wen, H. C. Wu, J. Aimi, C. C. Hung, Y. C. Chiang, C. C. Kuo and W. C. Chen, *Macromolecules*, 2017, **50**, 4982–4992.
104 G. N. Wang, L. Shaw, J. Xu, T. Kurosawa, B. C. Schroeder, J. Y. Oh, S. J. Benight and Z. Bao, *Adv. Funct. Mater.*, 2016, **26**, 7254–7262.
105 W. Zhao, T. Cao and J. M. White, *Adv. Funct. Mater.*, 2004, **14**, 783–790.
106 X. Yan, Z. Liu, Q. Zhang, J. Lopez, H. Wang, H. C. Wu, S. Niu, H. Yan, S. Wang, T. Lei, J. Li, D. Qi, P. Huang, J. Huang, Y. Zhang, Y. Wang, G. Li, J. B. H. Tok, X. Chen and Z. Bao, *J. Am. Chem. Soc.*, 2018, **140**, 5280–5289.
107 P. Song and H. Wang, *Adv. Mater.*, 2020, **32**, 1901244.
108 H. C. Wu, F. Lissel, G. J. N. Wang, D. M. Koshy, S. Nikzad, H. Yan, J. Xu, S. Luo, N. Matsuhisa, Y. Cheng, F. Wang, B. Ji, D. Li, W. C. Chen, G. Xue and Z. Bao, *Adv. Funct. Mater.*, 2021, **31**, 2009201.
109 G. J. N. Wang, Y. Zheng, S. Zhang, J. Kang, H. C. Wu, A. Gasperini, H. Zhang, X. Gu and Z. Bao, *Chem. Mater.*, 2019, **31**, 6465–6475.
110 F. J. Kahle, C. Saller, A. Köhler and P. Strohriegl, *Adv. Energy Mater.*, 2017, **7**, 1700306.
111 Y. Zheng, G. J. N. Wang, J. Kang, M. Nikolka, H. C. Wu, H. Tran, S. Zhang, H. Yan, H. Chen, P. Y. Yuen, J. Mun, R. H. Dauskardt, I. McCulloch, J. B. H. Tok, X. Gu and Z. Bao, *Adv. Funct. Mater.*, 2019, **29**, 1905340.
112 M. U. Ocheje, M. Comı, R. Yang, Z. Chen, Y. Liu, N. Yousefi, M. Al-hashimi and S. Rondeau-gagne, *J. Mater. Chem. C*, 2022, **10**, 4236–4246.
113 H. C. Wu, C. C. Hung, C. W. Hong, H. S. Sun, J. T. Wang, G. Yamashita, T. Higashihara and W. C. Chen, *Macromolecules*, 2016, **49**, 8540–8548.
114 Y. C. Chiang, H. C. Wu, H. F. Wen, C. C. Hung, C. W. Hong, C. C. Kuo, T. Higashihara and W. C. Chen, *Macromolecules*, 2019, **52**, 4393–4404.
115 S. W. Sides, J. Curro, G. S. Grest, M. J. Stevens, T. Soddemann, A. Habenschuss and J. D. Londono, *Macromolecules*, 2002, **35**, 6455–6465.
116 J. E. Mark, *Acc. Chem. Res.*, 2004, **37**, 946–953.
117 N. Kamatham, O. A. Ibraikulov, P. Durand, J. Wang, O. Boyron, B. Heinrich, T. Heiser, P. Lévêque, N. Leclerc and S. Méry, *Adv. Funct. Mater.*, 2020, **31**, 2007734.
118 Y. Ding, L. Jiang, Y. Du, S. Kim, X. Wang, H. Lu, G. Zhang, K. Cho and L. Qiu, *Chem. Commun.*, 2020, **7**, 11867–11870.
119 Y. Ding, Y. Zhu, X. Wang, Y. Wang, S. Zhang, G. Zhang, X. Gu and L. Qiu, *Chem. Mater.*, 2022, **34**, 2696–2707.
120 G. Xue, X. Zhao, G. Qu, T. Xu, A. Gumyusenge, Z. Zhang, Y. Zhao, Y. Diao, H. Li and J. Mei, *ACS Appl. Mater. Interfaces*, 2017, **9**, 25426–25433.
121 Z. Wang, Z. Liu, L. Ning, M. Xiao, Y. Yi, Z. Cai, A. Sadhanala, G. Zhang, W. Chen, H. Sirringhaus and D. Zhang, *Chem. Mater.*, 2018, **30**, 3090–3100.
122 Y. C. Lin, F. H. Chen, Y. C. Chiang, C. C. Chueh and W. C. Chen, *ACS Appl. Mater. Interfaces*, 2019, **11**, 34158–34170.
123 H. C. Yen, Y. C. Lin and W. C. Chen, *Macromolecules*, 2021, **54**, 1665–1676.
124 A. Babel and S. A. Jenekhe, *Macromolecules*, 2004, **37**, 9835–9840.
125 L. Qiu, X. Wang, W. H. Lee, J. A. Lim, J. S. Kim, D. Kwak and K. Cho, *Chem. Mater.*, 2009, **21**, 4380–4386.
126 J. I. Scott, X. Xue, M. Wang, R. J. Kline, B. C. Ho, D. Dougherty, C. Zhou, G. Bazan and B. T. O'Connor, *ACS Appl. Mater. Interfaces*, 2016, **8**, 14037–14045.
127 N. Onojima, N. Akiyama, Y. Mori, T. Sugai and S. Obata, *Org. Electron.*, 2020, **78**, 105597.
128 Q. Y. Yan, Y. W. Shia, D. Y. Guo and W. Y. Lee, *Macromol. Res.*, 2020, **28**, 660–669.
129 S. G. Lee, H. S. Lee, S. Lee, C. W. Kim and W. H. Lee, *Org. Electron.*, 2015, **24**, 113–119.
130 J. Xu, S. Wang, G. N. Wang, C. Zhu, S. Luo, L. Jin, X. Gu, S. Chen, V. R. Feig, J. W. F. To, S. Rondeau-gagné, J. Park, B. C. Schroeder, C. Lu, J. Y. Oh, Y. Wang, Y. Kim, H. Yan, R. Sinclair, D. Zhou, G. Xue, B. Murmann, C. Linder, W. Cai, J. B. Tok, J. W. Chung and Z. Bao, *Science*, 2017, **355**, 59–64.
131 F. Ge, S. Wei, Z. Liu, G. Wang, X. Wang, G. Zhang, H. Lu, K. Cho and L. Qiu, *ACS Appl. Mater. Interfaces*, 2018, **10**, 9602–9611.
132 A. R. Aiyar, J. Hong, R. Nambiar, D. M. Collard and E. Reichmanis, *Adv. Funct. Mater.*, 2011, **21**, 2652–2659.
133 D. Choi, M. Chang and E. Reichmanis, *Adv. Funct. Mater.*, 2015, **25**, 920–927.
134 G. Zhang, M. Mcbride, N. Persson, S. Lee, T. J. Dunn, M. F. Toney, Z. Yuan, Y. Kwon, P. Chu, B. Risteen and E. Reichmanis, *Chem. Mater.*, 2017, **29**, 7645–7652.
135 E. Song, B. Kang, H. H. Choi, D. H. Sin, H. Lee, W. H. Lee and K. Cho, *Adv. Electron. Mater.*, 2016, **2**, 1500250.
136 D. Liu, Z. Ding, Y. Wu, S. F. Liu, Y. Han and K. Zhao, *Macromolecules*, 2022, **55**, 297–308.
137 C. J. Ellison and J. M. Torkelson, *Nat. Mater.*, 2003, **2**, 695–700.
138 C. M. Stafford, B. D. Vogt, C. Harrison, D. Julthongpiput and R. Huang, *Macromolecules*, 2006, **39**, 5095–5099.
139 J. L. Keddie, R. A. L. Jones and R. A. Cory, *Europhys. Lett.*, 1994, **27**, 59–64.
140 B. Park, H. Kang, Y. H. Ha, J. Kim, J. Lee, K. Yu, S. Kwon, S. Jang, S. Kim, S. Jeong, S. Hong, S. Byun, S. Kwon, Y. Kim and K. Lee, *Adv. Sci.*, 2021, **8**, 2100332.
141 Y. Yang and M. W. Urban, *Chem. Soc. Rev.*, 2013, **42**, 7446–7467.
142 J. Dahlke, S. Zechel, M. D. Hager and U. S. Schubert, *Adv. Mater. Interfaces*, 2018, **5**, 1800051.
143 S. Wang and M. W. Urban, *Nat. Rev. Mater.*, 2020, **5**, 562–583.
144 L. Laysandra, C. H. Chuang, S. Kobayashi, A. N. Au-Duong, Y. H. Cheng, Y. T. Li, M. M. Mburu, T. Isono, T. Satoh and Y. C. Chiu, *ACS Appl. Polym. Mater.*, 2020, **2**, 5432–5443.
145 F. Song, Z. Li, P. Jia, M. Zhang, C. Bo, G. Feng, L. Hu and Y. Zhou, *J. Mater. Chem. A*, 2019, **7**, 13400–13410.
146 S. C. Cummings, O. J. Dodo, A. C. Hull, B. Zhang, C. P. Myers, J. L. Sparks and D. Konkolewicz, *ACS Appl. Polym. Mater.*, 2020, **2**, 1108–1113.

147 J. F. Mei, X. Y. Jia, J. C. Lai, Y. Sun, C. H. Li, J. H. Wu, Y. Cao, X. Z. You and Z. Bao, *Macromol. Rapid Commun.*, 2016, **37**, 1667–1675.
148 C. H. Li and J. L. Zuo, *Adv. Mater.*, 2020, **32**, 1903762.
149 Y. L. Rao, A. Chortos, R. Pfattner, F. Lissel, Y. C. Chiu, V. Feig, J. Xu, T. Kurosawa, X. Gu, C. Wang, M. He, J. W. Chung and Z. Bao, *J. Am. Chem. Soc.*, 2016, **138**, 6020–6027.
150 G. Sinawang, M. Osaki, Y. Takashima, H. Yamaguchi and A. Harada, *Chem. Commun.*, 2020, **56**, 4381–4395.
151 Y. Wang, X. Huang and X. Zhang, *Nat. Commun.*, 2021, **12**, 1291.
152 Z. Q. Lei, P. Xie, M. Z. Rong and M. Q. Zhang, *J. Mater. Chem. A*, 2015, **3**, 19662–19668.
153 C. Mo, L. Xiang and Y. Chen, *Macromol. Rapid Commun.*, 2021, **42**, 2100025.
154 C. Ouyang, C. Zhao, W. Li, X. Wu, X. Le, T. Chen, W. Huang, Q. Gao, X. Shan, R. Zhg and W. Zhang, *Macromol. Mater. Eng.*, 2020, **305**, 2000089.
155 Y. Li, L. Yang, Y. Zeng, Y. Wu, Y. Wei and L. Tao, *Chem. Mater.*, 2019, **31**, 5576–5583.
156 S. Shan, D. Mai, Y. Lin and A. Zhang, *ACS Appl. Polym. Mater.*, 2021, **3**, 5115–5124.
157 R. P. Wool and K. M. O'Connor, *J. Appl. Phys.*, 1981, **52**, 5953.
158 R. P. Wool, *Soft Matter*, 2008, **4**, 400–418.
159 X. Chen, J. Zhu, Y. Luo, J. Chen, X. Ma, D. Bukhvalov, H. Liu, M. Zhang and Z. Luo, *Phys. Chem. Chem. Phys.*, 2020, **22**, 17620–17631.
160 J. Kang, D. Son, G. J. N. Wang, Y. Liu, J. Lopez, Y. Kim, J. Y. Oh, T. Katsumata, J. Mun, Y. Lee, L. Jin, J. B. H. Tok and Z. Bao, *Adv. Mater.*, 2018, **30**, 1706846.
161 Y. L. Liu and T. W. Chuo, *Polym. Chem.*, 2013, **4**, 2194–2205.
162 Y. He, S. Liao, H. Jia, Y. Cao, Z. Wang and Y. Wang, *Adv. Mater.*, 2015, **27**, 4622–4627.
163 V. K. Thakur and M. R. Kessler, *Polymer*, 2015, **69**, 369–383.
164 M. U. Ocheje, M. Selivanova, S. Zhang, T. H. Van Nguyen, B. P. Charron, C. H. Chuang, Y. H. Cheng, B. Billet, S. Noori, Y. C. Chiu, X. Gu and S. Rondeau-Gagné, *Polym. Chem.*, 2018, **9**, 5531–5542.
165 C. H. Li, C. Wang, C. Keplinger, J. L. Zuo, L. Jin, Y. Sun, P. Zheng, Y. Cao, F. Lissel, C. Linder, X. Z. You and Z. Bao, *Nat. Chem.*, 2016, **8**, 618–624.
166 S. Zhang, Y. H. Cheng, L. Galuska, A. Roy, M. Lorenz, B. Chen, S. Luo, Y. T. Li, C. C. Hung, Z. Qian, P. B. J. St. Onge, G. T. Mason, L. Cowen, D. Zhou, S. I. Nazarenko, R. F. Storey, B. C. Schroeder, S. Rondeau-Gagné, Y. C. Chiu and X. Gu, *Adv. Funct. Mater.*, 2020, **30**, 2000663.
167 S. Zhang and F. Cicoira, *Adv. Mater.*, 2017, **29**, 1703098.
168 S. Zhang, Y. Li, G. Tomasello, M. Anthonisen, X. Li, M. Mazzeo, A. Genco, P. Grutter and F. Cicoira, *Adv. Electron. Mater.*, 2019, **5**, 1900191.
169 Y. Li, S. Zhang, X. Li, V. R. N. Unnava and F. Cicoira, *Flex. Print. Electron.*, 2019, **4**, 044004.
170 Y. Li, S. Zhang, N. Hamad, K. Kim, L. Liu, M. Lerond and F. Cicoira, *Macromol. Biosci.*, 2020, **20**, 2000146.
171 Y. Li, X. Li, S. Zhang, L. Liu, N. Hamad, S. R. Bobbara, D. Pasini and F. Cicoira, *Adv. Funct. Mater.*, 2020, **30**, 2002853.
172 X. Zhou, A. Rajeev, A. Subramanian, Y. Li, N. Rossetti, G. Natale, G. A. Lodygensky and F. Cicoira, *Acta Biomater.*, 2022, **139**, 296–306.
173 Y. Li, X. Zhou, B. Sarkar, N. Gagnon-Lafrenais and F. Cicoira, *Adv. Mater.*, 2022, **34**, 2108932.
174 H. Chen, Y. Guo, G. Yu, Y. Zhao, J. Zhang, D. Gao, H. Liu and Y. Liu, *Adv. Mater.*, 2012, **24**, 4618–4622.
175 Y. Zhao, X. Zhao, M. Roders, A. Gumyusenge, A. L. Ayzner and J. Mei, *Adv. Mater.*, 2017, **29**, 1605056.
176 Z. Qian, Z. Cao, L. Galuska, S. Zhang, J. Xu and X. Gu, *Macromol. Chem. Phys.*, 2019, **220**, 1900062.
177 Y. Li, W. K. Tatum, J. W. Onorato, S. D. Barajas, Y. Y. Yang and C. K. Luscombe, *Polym. Chem.*, 2017, **8**, 5185–5193.
178 H. Wen, H. Wu, J. Aimi, C. Hung, Y. Chiang, C. Kuo and W. Chen, *Macromolecules*, 2017, **50**, 4982–4992.
179 M. Shin, J. Y. Oh, K.-E. Byun, Y.-J. Lee, B. Kim, H.-K. Baik, J.-J. Park and U. Jeong, *Adv. Mater.*, 2015, **27**, 1255–1261.
180 F. Sugiyama, A. T. Kleinschmidt, L. V. Kayser, M. A. Alkhadra, J. M. Wan, A. S. Chiang, D. Rodriquez, S. E. Root, S. Savagatrup and D. J. Lipomi, *Macromolecules*, 2018, **51**, 5944–5949.
181 H. Wu, C. Hung, C. Hong, H. Sun, J. Wang, G. Yamashita, T. Higashihara and W. Chen, *Macromolecules*, 2016, **49**, 8540–8548.
182 M. J. Powell, *IEEE Trans. Electron Devices*, 1989, **36**, 2753–2763.
183 C.-S. Yang, L. L. Smith, C. B. Arthur and G. N. Parsons, *J. Vac. Sci. Technol., B: Microelectron. Nanometer Struct.--Process., Meas., Phenom.*, 2000, **18**, 683.
184 K. H. Cherenack, A. Z. Kattamis, B. Hekmatshoar, J. C. Sturm and S. Wagner, *Mater. Res. Soc. Symp. Proc.*, 2008, **1066**, 10662003.
185 D. Son, J. Kang, O. Vardoulis, Y. Kim, N. Matsuhisa, J. Y. Oh, J. W. To, J. Mun, T. Katsumata, Y. Liu, A. F. McGuire, M. Krason, F. Molina-Lopez, J. Ham, U. Kraft, Y. Lee, Y. Yun, J. B. H. Tok and Z. Bao, *Nat. Nanotechnol.*, 2018, **13**, 1057–1065.
186 B. C. K. Tee, C. Wang, R. Allen and Z. Bao, *Nat. Nanotechnol.*, 2012, **7**, 825–832.
187 J. Zhao, L. Sun, Z. Chu, T. Li, F. Zhang, L. Li and W. Zhang, *AIP Adv.*, 2020, **10**, 035020.